

AD-A185 657 FLIGHT MODEL DISCHARGE SYSTEM(U) HUGHES RESEARCH LABS  
MALIBU CA R R ROBSON ET AL. APR 87 SCIENTIFIC-3  
AFGL-TR-87-0143 F19628-83-C-0143

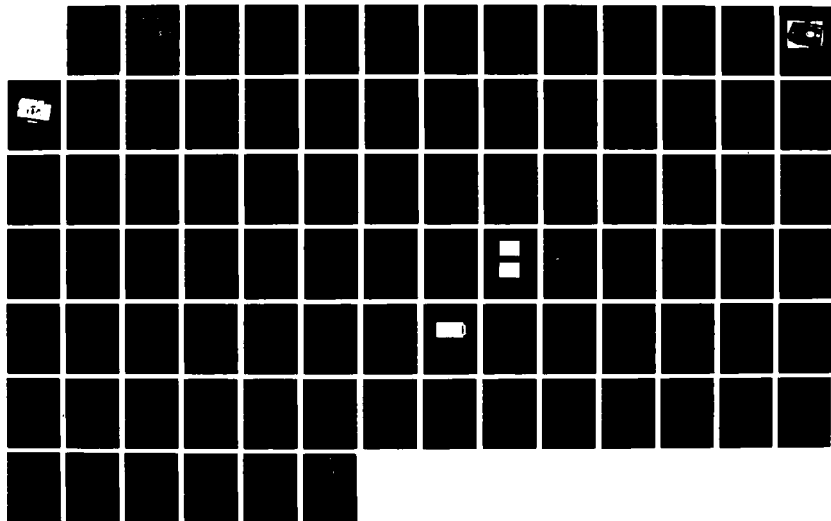
AD-A185 657 FLIGHT MODEL DISCHARGE SYSTEM(U) HUGHES RESEARCH LABS  
MALIBU CA R R ROBSON ET AL. APR 87 SCIENTIFIC-3  
AFGL-TR-87-0143 F19628-83-C-0143

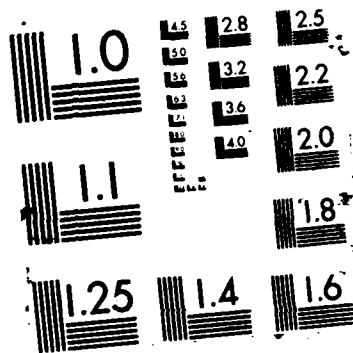
1/1

**UNCLASSIFIED**

F/G 22/2

NL





DTIC FILE COPY

(12)

# FLIGHT MODEL DISCHARGE SYSTEM

AD-A185 657

R.R. Robson, W.S. Williamson, and J. Santoru

Hughes Research Laboratories  
3011 Malibu Canyon Road  
Malibu, CA 90265

April 1987

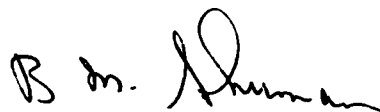
Scientific Report No. 3

DTIC  
ELECTE  
OCT 15 1987  
S D

*Approved for public release; distribution unlimited.*


Prepared for  
AIR FORCE GEOPHYSICS LABORATORY  
Air Force Systems Command  
United States Air Force  
Hanscom AFB, MA 01731

"This technical report has been reviewed and is approved for publication"



(Signature)

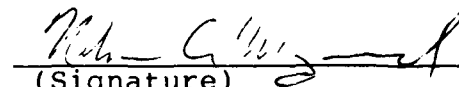
B.M. SHUMAN  
Contract Manager



(Signature)

for JOHN A. GAUDET, Lt Col, USAF  
Branch Chief

FOR THE COMMANDER



(Signature)

for RITA C. SAGALYN  
Division Director

This report has been reviewed by the ESD Public Affairs Office (PA) and is releasable to the National Technical Information Service (NTIS).

Qualified requestors may obtain additional copies from the Defense Technical Information Center. All others should apply to the National Technical Information Service.

If your address has changed, or if you wish to be removed from the mailing list, or if the addressee is no longer employed by your organization, please notify AFGL/DAA, Hanscom AFB, MA 01731. This will assist us in maintaining a current mailing list.

Do not return copies of this report unless contractual obligations or notices on a specific document requires that it be returned.

UNCLASSIFIED

SECURITY CLASSIFICATION OF THIS PAGE

AD-A185657

## REPORT DOCUMENTATION PAGE

Form Approved  
OMB No. 0704-0188

1a. REPORT SECURITY CLASSIFICATION Unclassified			1b. RESTRICTIVE MARKINGS		
2a. SECURITY CLASSIFICATION AUTHORITY			3. DISTRIBUTION/AVAILABILITY OF REPORT Approved for public release; distribution unlimited.		
2b. DECLASSIFICATION/DOWNGRADING SCHEDULE					
4. PERFORMING ORGANIZATION REPORT NUMBER(S)			5. MONITORING ORGANIZATION REPORT NUMBER(S) AFGL-TR-87-0143		
6a. NAME OF PERFORMING ORGANIZATION Hughes Research Labs		6b. OFFICE SYMBOL (if applicable)	7a. NAME OF MONITORING ORGANIZATION Air Force Geophysics Laboratory		
6c. ADDRESS (City, State, and ZIP Code) 3011 Malibu Canyon Road Malibu, CA 90265			7b. ADDRESS (City, State, and ZIP Code) Hanscom AFB Massachusetts 01731		
8a. NAME OF FUNDING/SPONSORING ORGANIZATION Air Force Geophysics Lab.		8b. OFFICE SYMBOL (if applicable) AFGL/PHE	9. PROCUREMENT INSTRUMENT IDENTIFICATION NUMBER F19628-83-C-0143		
8c. ADDRESS (City, State, and ZIP Code) Hanscom AFB Massachusetts 01731			10. SOURCE OF FUNDING NUMBERS		
			PROGRAM ELEMENT NO 63410F	PROJECT NO 2823	TASK NO 01
			WORK UNIT ACCESSION NO AA		
11. TITLE (Include Security Classification) Flight Model Discharge System					
12. PERSONAL AUTHOR(S) R.R. Robson, W.S. Williamson, and J. Santoru					
13a. TYPE OF REPORT Scientific Report 3		13b. TIME COVERED FROM 12/85 to 2/87	14. DATE OF REPORT (Year, Month, Day) April 1987		15. PAGE COUNT 95
16. SUPPLEMENTARY NOTATION					
17. COSATI CODES			18. SUBJECT TERMS (Continue on reverse if necessary and identify by block number)		
FIELD	GROUP	SUB-GROUP	Spacecraft charging, FMDS, Spacecraft automatic active discharge system, Flight model discharge system		
19. ABSTRACT (Continue on reverse if necessary and identify by block number)					
<p>The Flight Model Discharge System (FMDS) Program has completed its third year. The FMDS is a spacecraft charge-control system designed to overcome the problem of charge buildup on a space vehicle which occurs during periods of adverse space environmental conditions. An overview of the FMDS system is presented, followed by an in-depth treatment of the significant technical developments that have occurred during the past year. The major areas covered include the plasma generator lifetest and the system thermal analysis.</p>					
20. DISTRIBUTION/AVAILABILITY OF ABSTRACT <input type="checkbox"/> UNCLASSIFIED UNLIMITED <input checked="" type="checkbox"/> SAME AS RPT <input type="checkbox"/> DTC USERS			21. ABSTRACT SECURITY CLASSIFICATION Unclassified		
22a. NAME OF RESPONSIBLE INDIVIDUAL Bert Shuman			22b. TELEPHONE (Include Area Code) (617) 377-3991		22c. OFFICE SYMBOL AFGL/PHE

DD Form 1473, JUN 86

Previous editions are obsolete

SECURITY CLASSIFICATION OF THIS PAGE

Unclassified

## TABLE OF CONTENTS

SECTION	PAGE
1 INTRODUCTION.....	1
2 FLIGHT MODEL DISCHARGE SYSTEM TOTAL SYSTEM.....	3
2.1 Overall System.....	5
2.2 Components.....	11
3 ELECTROSTATIC ANALYZERS.....	23
4 SURFACE POTENTIAL MONITORS.....	25
4.1 Basic SPM Design.....	25
4.2 SPM Design Considerations.....	26
5 TRANSIENT PULSE MONITOR.....	29
6 CONTROLLER.....	33
7 PLASMA SOURCE.....	37
7.1 Plasma Generator Design.....	37
7.2 Test Results.....	40
7.3 Contamination Measurements.....	48
7.4 Magnetic Field Measurements.....	53
8 SYSTEM THERMAL ANALYSIS.....	55
8.1 Analysis Inputs.....	55
8.2 Operating Conditions.....	63
8.3 Assumptions.....	68
8.4 Analysis Method.....	69
8.5 Results.....	69
8.6 FMDS System Design.....	76
8.7 Discussion and Recommendations.....	83
9 CONCLUSIONS.....	85
REFERENCES.....	87

# LIST OF ILLUSTRATIONS

FIGURE		PAGE
2-1	Block diagram of the FMDS.....	4
2-2	Model of the FMDS with its cover in place.....	6
2-3	Model of the FMDS with its cover removed.....	7
2-4	Flight design layout of the FMDS.....	8
2-5	Shift in the observed ion and electron spectra caused by environmental conditions conducive to charging and by actual charging of the spacecraft.....	12
2-6	Charging characteristics of a shaded dielectric sensor.....	13
4-1	Flight package design for the SPM.....	27
6-1	Successive approximation register A/D converter originally planned for FMDS.....	35
6-2	Counting type of A/D converter now planned for FMDS.....	36
7-1	Simple schematic of the plasma generator.....	39
7-2	Cross section of the flight plasma generator.....	41
7-3	Ion emission current characteristics of the plasma generator for various keeper and discharge current setpoints.....	44
7-4	Keeper and discharge voltages as a function of expellant flow rate.....	45
7-5	Keeper current and voltage during gas burst ignition.....	46
7-6	Plasma source voltages and ion emission during the first few minutes after starting.....	47
7-7	Positions of the contamination "witness" slides during the plasma generator lifetest.....	49
7-8	Optical transmission loss of contamination "witness" slide 3.....	51



A-1	
1	2
3	4
5	6
7	8
9	10

8-1	Flight Model Discharge System (FMDS).....	56
8-2	FMDS mounted near the antenna farm of a spin stabilized communications satellite.....	58
8-3	Cross section of a multiwire board.....	59
8-4	Typical multiwire board ground plane.....	60
8-5	Simplified thermal model of the FMDS.....	61
8-6	Typical enclosure/electronics-box/component thermal interface.....	62
8-7	Master microprocessor assembly component layout.....	64
8-8	TPM threshold detector assembly component layout.....	65
8-9	Plasma Generator Electronics (shelf 2) assembly component layout.....	66
8-10	FMDS power dissipation map.....	67
8-11	Detailed FMDS nodal map.....	70
8-12	Normalized radiator area versus $T_{HOT}$ for the conductive, radiative, and insulated connections with $T_M = 43^\circ\text{C}$ .....	72
8-13	Heater power versus $T_{COLD}$ for the conductive connection with $T_M = -13^\circ\text{C}$ .....	73
8-14	Heater power versus $T_{COLD}$ for the radiative connection with $T_M = -13^\circ\text{C}$ .....	74
8-15	Heater power versus $T_{COLD}$ for the case where FMDS is insulated from the satellite.....	75



## LIST OF TABLES

TABLE		PAGE
2-1	Summary of FMDS weights.....	10
2-2	Summary of FMDS power consumption.....	10
2-3	Electrostatic analyzer contractual specifications and respective flight design parameters.....	15
2-4	Surface potential monitor contractual specifications and respective flight design parameters.....	16
2-5	Transient pulse monitor contractual specifications and respective flight design parameters.....	17
2-6	Controller contractual specifications and respective flight design parameters.....	18
2-7	Plasma source contractual specifications and respective flight design parameters.....	19
2-8	FMDS system contractual specifications and respective flight design parameters.....	20
7-1	SPACECLAMP plasma generator characteristics.....	38
8-1	TPM threshold detector assembly steady state component operating temperatures.....	77
8-2	Plasma generator electronics (shelf 2) assembly steady state component operating temperatures.....	80
8-3	Master microprocessor assembly steady state component operating temperatures.....	81

## SECTION 1

### INTRODUCTION

The objectives of the FMDS program are to design, develop, fabricate, test, and deliver two flight units of a satellite Flight Model Discharge System (FMDS). The FMDS is a stand-alone system capable of autonomous operation (except for power) that will monitor spacecraft potential, determine when spacecraft charging is present, and operate a discharge device to eliminate potentials and maintain the spacecraft in a neutral charge state. The FMDS is designed to be incorporated into the "housekeeping" function of any spacecraft which may be subject to spacecraft charging. While full ground-command capability is retained for redundancy, only a "power on" command is required to activate the system. In addition to the capability for remote command override of its autonomous operation, the FMDS also provides telemetry signals to monitor such functions as sensor outputs, controller "commands," plasma source operation, gas supply in the reservoir tank, and system state-of-health diagnostics, e.g., temperatures, voltages, and currents.

In the following technical discussion, we present the results of the third year's effort on the FMDS contractual program, which is being carried out at Hughes Research Laboratories in Malibu, California. An overview of the FMDS system is presented, followed by an in-depth treatment of the significant technical developments that have occurred during the past year. For an in-depth discussion of the operation and capabilities of the FMDS system, refer to Scientific Report No. 2.<sup>1</sup>

## SECTION 2

### FLIGHT MODEL DISCHARGE SYSTEM TOTAL SYSTEM

The FMDS is a stand-alone system capable of autonomous operation (except for power) that monitors space-vehicle potential, determines when charging is present, and operates a discharge device to eliminate charge build-up and maintain the vehicle in a neutral charge state. The FMDS is designed to be incorporated into the "housekeeping" functions of any vehicle which may be subject to spacecraft charging. While full ground-command capability is retained for redundancy, only a "power on" command is required to activate the system. It detects charging, operates to neutralize the charging, and returns to the passive mode when the charging hazard is no longer present.

The FMDS consists of three types of components:

(1) Charging sensors:

- Electrostatic Analyzers (ESAs). These sensors detect absolute charging relative to the ambient plasma in space.
- Surface Potential Monitors (SPMs). These sensors determine differential charging relative to spacecraft ground.
- Transient Pulse Monitor (TPM). This sensor detects the electromagnetic pulses generated by the onset of arcing.

(2) An active discharge device (plasma source).

(3) A control unit to interpret the sensor outputs, determine when and if charging is occurring, and control the discharge device.

A block diagram of the system is shown in Figure 2-1.

The controller incorporates comprehensive charging-detection algorithms which contain ground-alterable parameters to allow in-space refinement of FMDS operation. The controller incorporates redundant and fault-tolerant software to permit the FMDS to continue operation in the face of specific faults or failures. In addition it has the capability for ground or remote-command

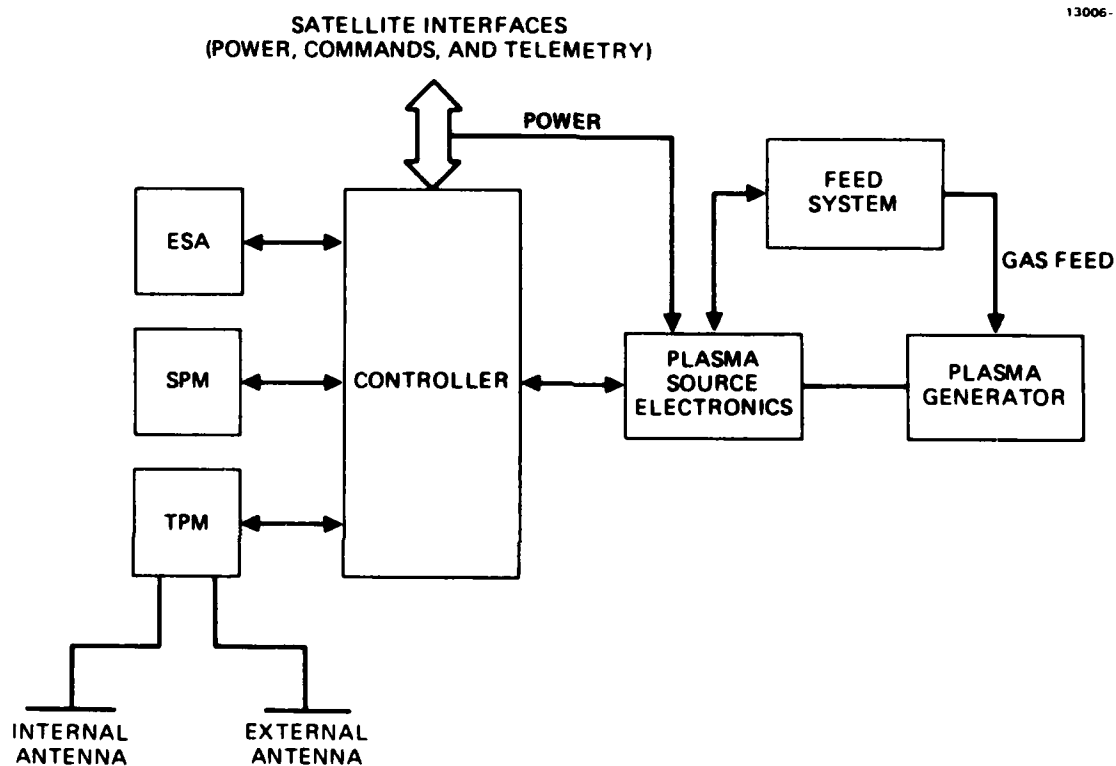


Figure 2-1. Block diagram of the FMDS.

override of its autonomous operation, and also provides telemetry signals to monitor such functions as sensor outputs, controller status flags, plasma source operation, gas supply pressure in the reservoir tank, temperatures, voltages, currents, etc.

The FMDS is ultimately intended for extended satellite operation at geosynchronous orbit; however, it is designed to withstand the launch and operating environments of both geosynchronous and Shuttle orbits. While the primary emphases are safety and reliability, low operating and transient voltages are also considered to avoid Paschen breakdown and to minimize EMI.

## 2.1 OVERALL SYSTEM

The general FMDS configuration is depicted in Figures 2-2 and 2-3. All components of the system are attached to a common honeycomb-structure mounting plate to provide a simple lightweight and structurally sturdy interface with the host spacecraft. No attempt is made in this model to indicate the exact interface of the FMDS with the host spacecraft since at this time a specific ride has not been determined. Because of this uncertainty, the FMDS has been designed so that it functions independently of the characteristics of the host spacecraft. The structurally integrated design approach will also facilitate system testing in both laboratory vacuum chambers and environmental test fixtures (vibration, thermal/vacuum, etc.).

The layout of the system has been slightly modified from the model shown in Figures 2-2 and 2-3; the new layout is shown in Figure 2-4. Alterations include an exchange of the ion and electron electrostatic analyzers (ESAs) and one surface potential monitor (SPM); an increase in the size of the xenon tank from 1 to 2 liters; and the moving of the plasma generator outside the cover. The ESAs and the SPM have been interchanged to move the entrance apertures on the ESAs further from the plasma generator, the size of the xenon tank has been increased to handle the

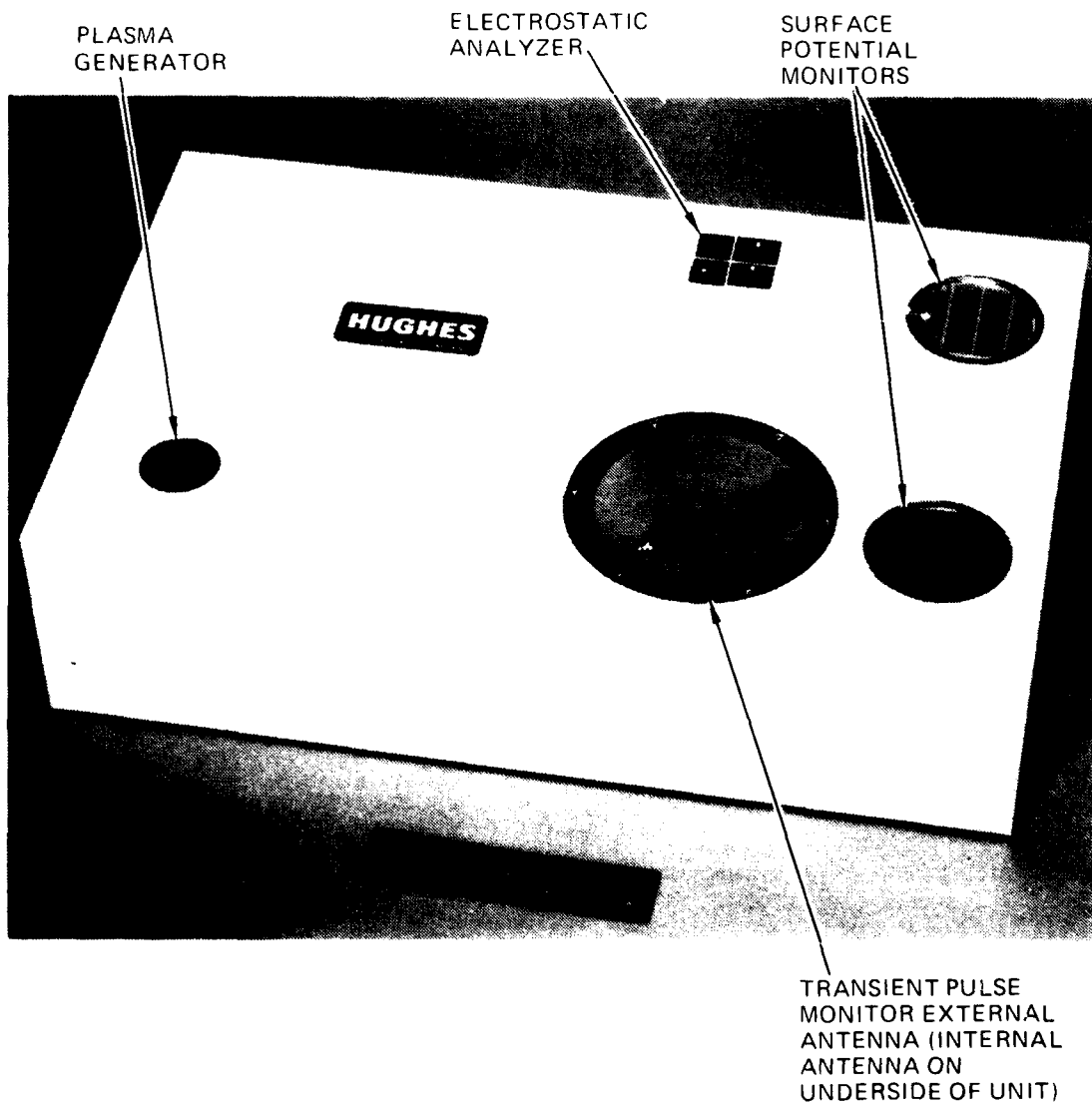


Figure 2-2. Model of the FMDS with its cover in place.

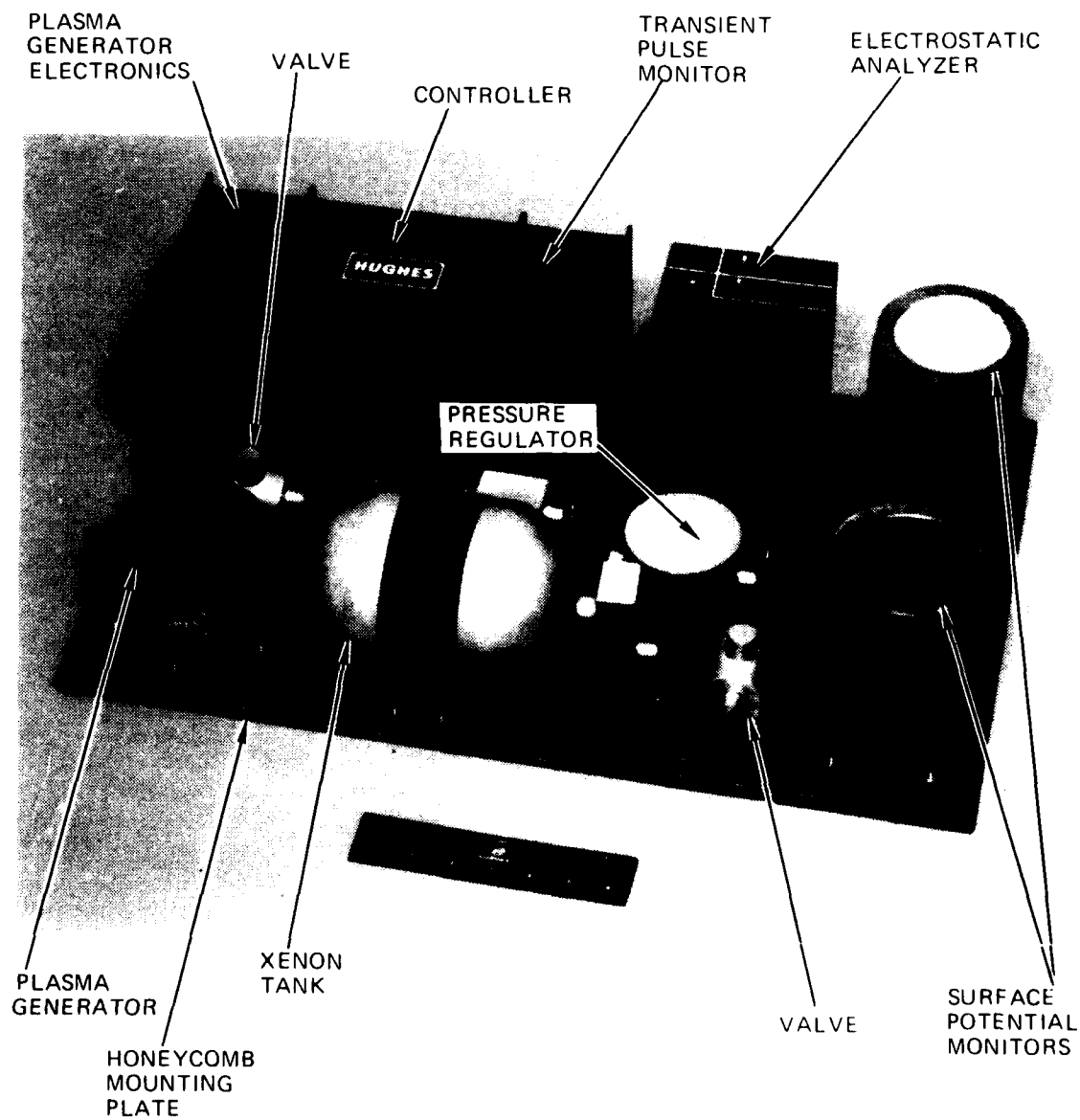


Figure 2-3. Model of the FMDS with its cover removed.

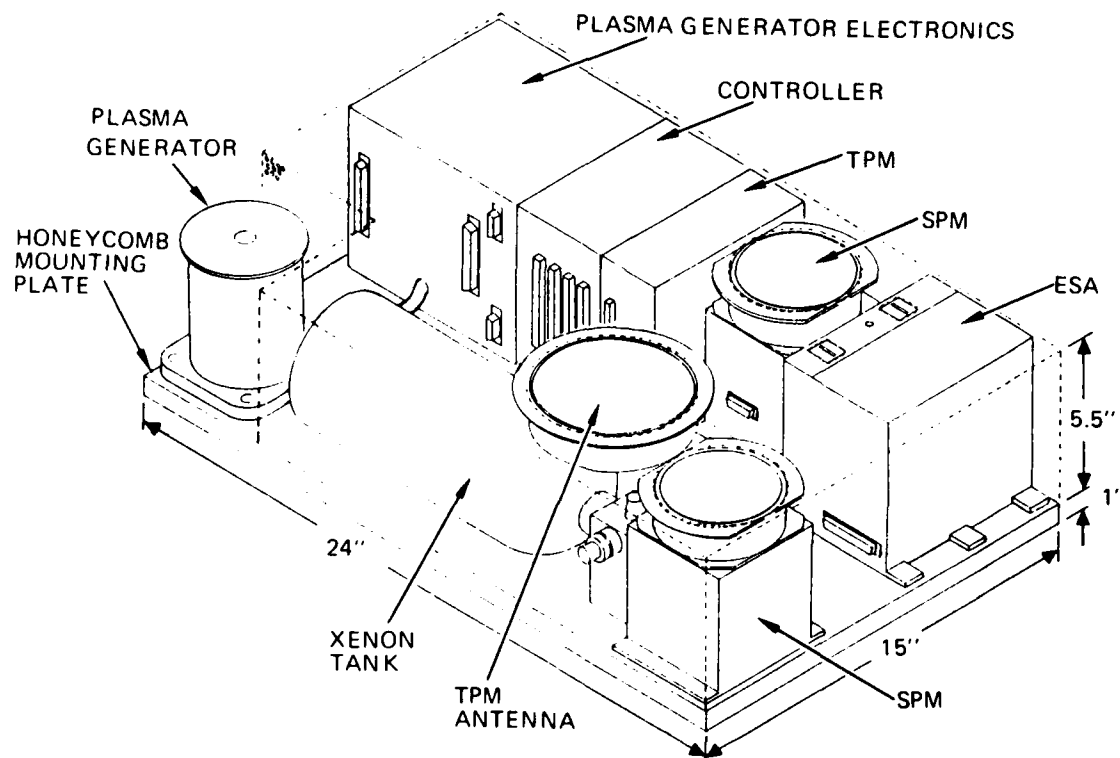


Figure 2-4. Flight design layout of the FMDS.



quantity of expellant required, and the plasma generator has been removed from inside the cover to prevent it from radiating heat to the electronics boxes.

Because of the diversity of functions required of the various FMDS components, each element is packaged separately and attached separately to the common mounting plate. Maintaining separation between each of the components has the added advantage of substituting of upgraded component designs if such upgrades become available in the future.

The two SPMs and the ESAs are mounted on one end of the FMDS mounting plate to provide both maximal and similar exposure of the sensors to incoming particle flux while avoiding (as much as possible) any local distortions of electrostatic equipotentials which might be caused by other devices such as the plasma source.

The plasma source is located at the other end of the FMDS where it is farthest from the charged-particle entrance apertures of the ESAs; this will minimize the introduction of plasma-source-generated particles. In this location, the source is reasonably remote from both the ESAs and the SPMs.

The electronics packages for the plasma-generator, TPM, and controller; the SPMs; the ESAs; and the plasma generator are all at the same height. This allows a cover to be added to the FMDS to form a ground plane and to provide a mounting surface for the TPM external antenna. Thermal control surfaces and/or thermal blankets will also be attached to the cover.

Inasmuch as the FMDS is intended for satellite use, minimizing weight, volume, and power is of utmost concern. The overall FMDS is expected to weigh less than 19.4 kg (42.4 lb.), and consume less than 13.7 W when the plasma source is not activated, and less than 28.1 W when it is activated. FMDS weights and power consumption are summarized in Tables 2-1 and 2-2 respectively. The overall dimensions are 16.5 x 38.1 x 61 cm (6.5 x 15 x 24 in.).

Table 2-1. Summary of FMDS Weights

15806-46

UNIT	MASS, kg	WEIGHT, lb	CONTRACT SPEC, lb
ESA	2.7	6.0	6.0
SPM (2 UNITS)	1.4	3.0	3.0
TPM	1.6	3.5	3.0
CONTROLLER	1.7	3.7	-
PLASMA SOURCE	1.4	3.0	15.0
SOURCE ELECTRONICS	2.0	4.4	
FEED SYSTEM	4.2	9.2	
HARNESS	0.7	1.5	-
THERMAL CONTROL	0.9	2.0	-
ENCLOSURE	2.2	4.8	-
FMDS DRY MASS	18.8	41.1	-
XENON	0.6	1.3	-
FMDS AT LAUNCH	19.4	42.4	35.0

Table 2-2. Summary of FMDS Power Consumption

15806-46

UNIT	SOURCE OFF, W	SOURCE ON, W	CONTRACT SPEC, W
ESA	1.25	1.25	1.25
SPM (2 UNITS)	1.0	1.0	2.0
TPM	4.0	4.0	3.0
CONTROLLER	4.0	4.0	(4.0)
PLASMA SOURCE	0.0	13.7	(25.0)
HOUSEKEEPING INVERTER	3.4	4.1	-
FMDS	13.7	28.1	
FMDS CONTRACT SPEC	10.0	35.0	

( ) = INFERRED

## 2.2 COMPONENTS

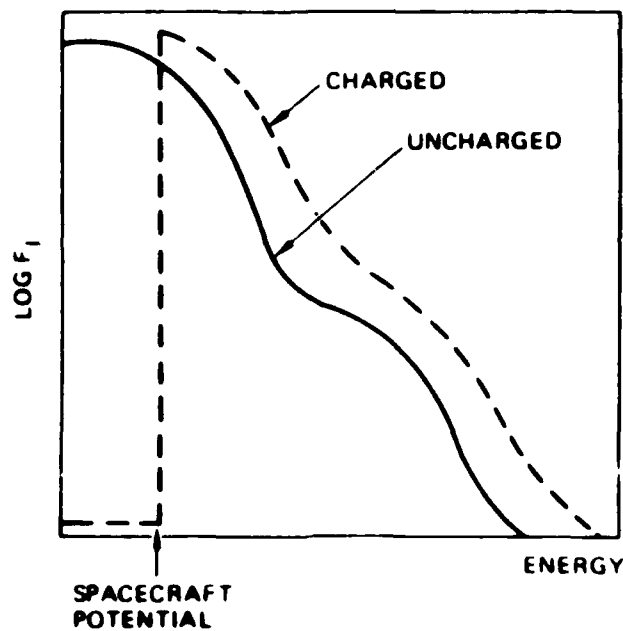
The ESAs will measure the energy distribution (from 50 eV to 20 keV) of the particles incident upon the satellite. There will be a shift in this energy distribution when the environmental conditions are conducive to spacecraft charging (caused by a change in the environmental conditions), and another shift directly related to the potential of the satellite frame relative to the space potential. Since the ESAs are referenced to the satellite frame and the particles originate with energies relative to space potential, any change in the potential of the satellite frame will appear as a change in the particle energy distributions. Algorithms in the controller will detect the shift in the particle energy distributions (Figure 2 5) in order to (1) provide an early warning that the environmental conditions are conducive to spacecraft charging (by detection of electrons), and (2) detect that charging of the satellite frame has exceeded a threshold level (by ion detection) and provide a signal to turn on the plasma source.

The SPMs will detect the onset of differential charging of the satellite dielectric surfaces. When the satellite is in sunlight and charging conditions exist, the isolated dielectric surfaces that are shaded will charge much faster than the satellite frame because of the lack of photo emission from these shaded surfaces (Figure 2 6). Therefore, by measuring the potential on the surface of a shaded dielectric sensor, differential charging can be detected quickly and prior to the detection of satellite frame charging by the ESA. When the satellite is in eclipse, however, satellite frame charging occurs faster than differential charging (Figure 2-6). In this circumstance the ESA will be the prime detector.

The TPM will detect electrical discharges that occur on the surface of the satellite resulting from differential charging. A floating plate sensor is employed to pick up radiated electric

# ION SPECTRUM

14881-16



# ELECTRON SPECTRUM

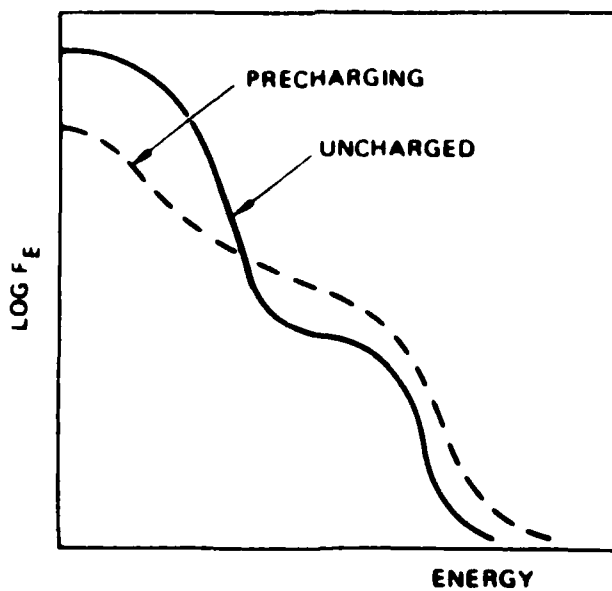


Figure 2-5. Shift in the observed ion and electron spectra caused by environmental conditions conducive to charging and by actual charging of the spacecraft.

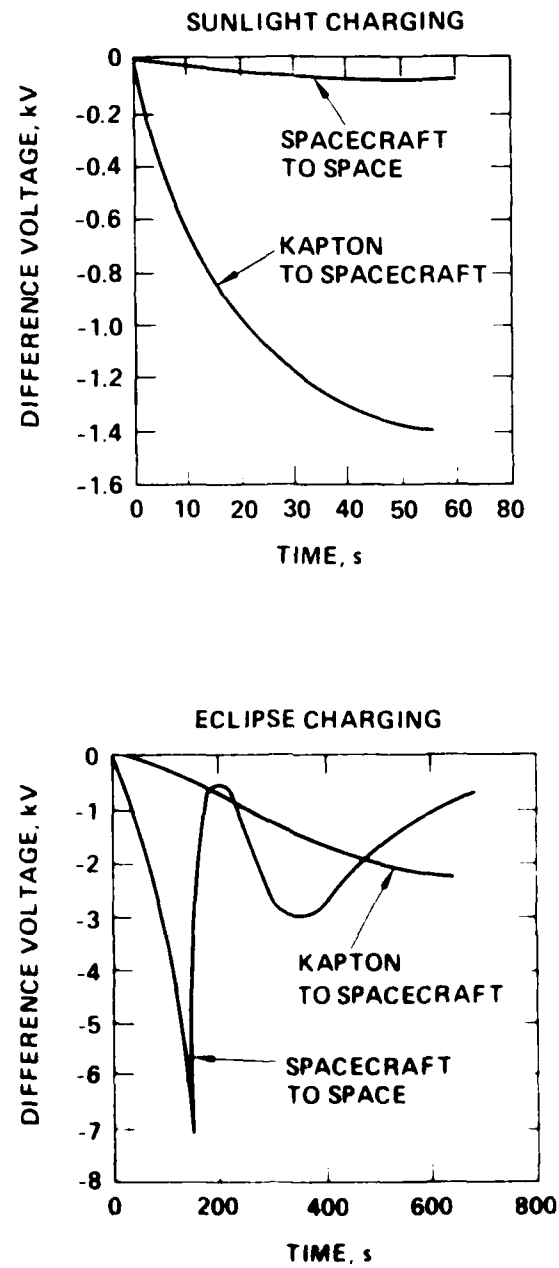


Figure 2 6. Charging characteristics of a shaded dielectric sensor.

fields caused by these discharges. If electrical discharges are occurring, it implies that the satellite is charged up, that the plasma generator should be turned on, and that the other sensors have failed to detect the charging. The TPM has ground-adjustable parameters and can be commanded to ignore transients which occur within 1 s following receipt of a command by the spacecraft. The TPM is designed to avoid false arc-discharging alarms.

The controller provides for autonomous control of the FMDS relative to the remainder of the satellite. It is also the device which ties the other units of the FMDS together. The brain of the controller is a microprocessor which contains the algorithms necessary to interpret the data from the sensors and command the plasma generator to turn ON when spacecraft charging is occurring, and then turn OFF when it is no longer required. The plasma generator is turned OFF after a programmable time-out (when the emission current from the plasma generator has been less than a threshold value for a specified period of time) and when the ambient electron environment returns to a quiescent condition. The controller also provides the command and telemetry interface with the satellite.

The plasma generator emits xenon ions and electrons in sufficient quantity ( $>1$  mA) to bathe the satellite in a conductive low energy ( $<50$  eV) plasma. This conductive plasma will drain the charge from dielectric surfaces and also form a "plasma bridge" to the surrounding natural space plasma environment. The plasma generator is capable of igniting in less than 1 s, operating for 1200 h, and executing 1000 ON/OFF cycles. It requires three power supplies and a gas feed system consisting of a xenon storage tank, a pressure regulator, valves, and a flow regulator.

Tables 2.3 through 2.8 list the major contractual specifications for the ESAs, SPMs, TPM, controller, plasma source, and system, respectively. The respective parameters of the flight design are also listed in these tables.

Table 2 3. Electrostatic Analyzer Contractual Specifications and Respective Flight Design Parameters

14881 1/1/84

CONTRACTUAL SPECS	DESIGN
ION AND ELECTRON SPECTRA < 100 eV TO 20 keV	50 eV TO 20 keV
GEOMETRIC FACTOR $\approx 10^{-5}$ TO $10^{-4}$ cm <sup>2</sup> SR	$6 \times 10^{-4}$ cm <sup>2</sup> SR
8 ENERGY CHANNELS	16 CHANNELS
2% OVERLAP AT FWHM	2% OVERLAP NO GAPS
SWEEPS OF 2, 5, AND 10 s	SWEEPS OF 4, 8, 16, AND 32 s
VOLTAGES SETTLED TO 95% BEFORE COUNTING	VOLTAGES SETTLED TO 95% BEFORE COUNTING
GRID TO REPEL PLASMA SOURCE IONS AND ELECTRONS (< 50 eV)	GRID BIASED AT 50 V
SUN SENSOR TO PROTECT CEM	SUN SENSOR
CMD OVERRIDE OF SUN SENSOR	CMD OVERRIDE
REDUCE UV SCATTERING	SANDBLASTED PLATES
COMMANDABLE CEM BIAS	COMMANDABLE BIAS (8 LEVELS)
THREE YEAR ON ORBIT LIFE	DESIGNED FOR THREE-YEAR OPERATIONAL LIFE
TELEMETRY	ACCUMULATED COUNTS, ENERGY CHANNEL STATUS, AND DIAGNOSTICS
1.25 W	1.25 W
6 lb	6 lb

Table 2-4. Surface Potential Monitor Contractual Specifications and Respective Flight Design Parameters

14881-1872

CONTRACTUAL SPECS	DESIGN
DIELECTRIC SURFACE POTENTIAL MEASURED WITH ELECTRIC FIELD SENSOR	VIBRATING ELECTRODE ELECTROSTATIC VOLTMETER
POTENTIAL AND POLARITY FROM 100 V TO 20 kV	DUAL RANGE: $\pm 2$ kV $\pm 20$ kV
TWO DIFFERENT DIELECTRICS IN FLIGHT	TWO INSTRUMENTS WITH DIFFERENT DIELECTRICS
CHOICE OF SIX DIFFERENT DIELECTRICS	CHANGE SENSING PLATE TO CHANGE DIELECTRICS
TELEMETRY	SURFACE POTENTIAL, RANGE, DIAGNOSTICS
$\leq 2$ W	$\leq 1$ W (2 UNITS)
$\leq 3$ lb	$\leq 3.5$ lb (2 UNITS)



Table 2-5. Transient Pulse Monitor Contractual Specifications and Respective Flight Design Parameters

CONTRACTUAL SPECS	DESIGN
DIPOLE SENSOR	MONOPOLE (123 cm <sup>2</sup> PLATE)
MEASURE RADIATED ELECTROMAGNETIC PULSES	MEASURE ELECTROSTATIC PULSES
MULTIPLE THRESHOLD LEVELS	8-BIT DAC
PARAMETERS MEASURED 1s	PARAMETERS MEASURED 4s
- MAX POSITIVE PEAK AMPLITUDE	- POSITIVE PEAK AMPLITUDE PULSE
- MAX NEGATIVE PEAK AMPLITUDE	- NEGATIVE PEAK AMPLITUDE PULSE
- POSITIVE INTEGRAL	- INTEGRALS NOT MEASURED
- NEGATIVE INTEGRAL	
- PULSE WIDTH	- PULSE WIDTH PULSE
- NUMBER OF PULSES	- PULSES 4s
10 V/m TO 10 kV/m FIELD STRENGTH	10 V/m TO 10 kV/m
10 ns TO 10 $\mu$ s PULSE WIDTHS	20 ns TO 10 $\mu$ s
1 COUNT ms MAX	1 COUNT 5ms
TELEMETRY	PARAMETERS MEASURED AND DIAGNOSTICS
3 W	4 W
3 lb	4 lb

**TABLE 2-6. Controller Contractual Specifications and Respective Flight Design Parameters.**

Contract Specs	Design
Provide autonomous operation of FMDS	Autonomous operation
Determine if threshold levels of charging have been exceeded	Charging above threshold will be detected
Turn on plasma source and operate for 5, 10, 30, or 60 min	Turn on and control plasma source. Turn off based on time (30, 60, 90, 120 min) and/or environmental conditions
Detect with 98% reliability <ul style="list-style-type: none"> <li>- 95% of cases for charging <math>&gt;500</math> V</li> <li>- 100% of cases for charging <math>&gt;1000</math> V</li> </ul>	Designed to meet based on SC9 data
Commandable threshold charging levels of 200, 500, 1000 and 2000 V	Same
Spacecraft arcing to activate plasma source	Arcing will activate plasma source
EMI pulses within 1 s of spacecraft command to be ignored	Ability to blank TPM for 1 s (requires signal from spacecraft)
External command adjustment of TPM algorithm	All algorithms will be adjustable via external command
External commanding of plasma source	Manual operation of complete FMDS
Telemetry	Status and diagnostics
Design to include considerations of radiation hardening	Hardened to $5 \times 10^5$ rads (flight)
Redundancy	Critical parameters stored in three locations (majority voting)
Excess capacity	Excess memory and I/O

Table 2-7. Plasma Source Contractual Specifications and Respective Flight Design Parameters

14881 20R3

CONTRACTUAL SPECS	DESIGN
<ul style="list-style-type: none"> <li>50 eV NEUTRAL PLASMA</li> <li>IONS FROM A NOBLE GAS</li> <li>10 <math>\mu</math>A, 100 <math>\mu</math>A, AND 1 mA ION CURRENT LEVELS (SELECTABLE)</li> <li>10s IGNITION</li> <li>1200 HOURS OPERATION</li> <li>1000 ON-OFF CYCLES</li> <li>25 W</li> <li>15 lb</li> <li>BLOW-OFF COVER</li> <li>TELEMETRY</li> </ul>	<ul style="list-style-type: none"> <li>40 eV</li> <li>90% XENON-10% HYDROGEN</li> <li>&lt; 200 <math>\mu</math>A TO &gt; 1 mA, 4 SETPOINTS FOR DISCHARGE AND KEEPER</li> <li>1s</li> <li>1200 hr</li> <li>1000 CYCLES</li> <li>10 W OPERATING</li> <li>20 W CONDITIONING</li> <li>&lt; 17 lb DRY</li> <li>REMOVE-BEFORE-LAUNCH COVER</li> <li>EMISSION CURRENT AND DIAGNOSTICS</li> </ul>

Table 2-8. FMDS System Contractual Specifications and Respective Flight Design Parameters

15866-44A

CONTRACTUAL SPECS	DESIGN
LOW-ENERGY PLASMA WITHIN 30s OF EXCEEDING A CHARGING THRESHOLD	SAME EXCEPT FOR ESA 16-s SWEEP WHICH REQUIRES 38s
ANALOG TELEMETRY OUTPUTS BETWEEN 0.00 AND 5.10V	NO ANALOG SIGNALS TO SATELLITE
DIGITAL COMMANDS AND TELEMETRY TTL COMPATIBLE	TTL COMPATIBLE AND OPTICALLY ISOLATED
ALL GROUND RETURNS SELF CONTAINED AND ISOLATED BY $\geq 1$ MEGOHM	DESIGNED TO MEET - SINGLE GROUND POINT PHILOSOPHY
PERMANENT MAGNETIC FIELDS $\leq 100$ nT AT 1 METER IN ANY DIRECTION	DESIGNED TO MEET
MATING CONNECTORS TO BE FURNISHED	MATING CONNECTORS WILL BE FURNISHED
NO CADMIUM-PLATED CONNECTORS OR OTHER HARDWARE	NO CADMIUM ANYWHERE
<35 LBS	41.1 LBS DRY 42.2 LBS AT LAUNCH
<10W WITH PLASMA SOURCE OFF	13.7W WITH SOURCE OFF 28.1W WITH SOURCE ON
POWER PROFILE TO BE PROVIDED	POWER PROFILE WILL BE MEASURED AND PROVIDED
HIGH-REL PARTS FOR >3 YR LIFE IN DEEP SPACE ORBIT	RAD-HARD CLASS-B PARTS
THERMAL MODELS TO BE PROVIDED	ANALYTICAL THERMAL MODELS WILL BE PROVIDED
MASS MODELS TO BE PROVIDED - BOTH ANALYTICAL MODELS AND HARDWARE SIMULATORS	ANALYTICAL MASS MODELS AND HARDWARE MASS SIMULATORS WILL BE PROVIDED
ELECTRICAL SIMULATORS TO BE PROVIDED	ELECTRICAL SIMULATORS WILL BE PROVIDED
GROUND SUPPORT EQUIPMENT TO BE PROVIDED - COMMAND/TELEMETRY AND POWER SOURCE	GROUND SUPPORT EQUIPMENT WILL BE PROVIDED - COMMAND/TELEMETRY, POWER SOURCE, AND VACUUM PUMP
EMI: DESIGNED TO MEET MIL-STD-461B AND MIL-STD-1541	DESIGNED TO MEET
SHALL MEET SHUTTLE SAFETY REQUIREMENTS - NASA HANDBOOK 1700.7A, JSC 11123 AND JSC 13830	DESIGNED TO MEET
ACCEPTANCE TESTS TO BE PERFORMED IN ACCORDANCE WITH MIL-STD-1540A	DESIGNED TO MEET
RANDOM VIBRATION:	DESIGNED TO MEET
FREQUENCY (Hz) PSD ( $g^2/Hz$ )	
20 0.004	
20-37.5 +12 dB/OCTAVE	
37.5-90 0.050	
90-200 +4 dB/OCTAVE	

(Continued)

**TABLE 2-8. FMDS System Contractual Specifications and Respective Flight Design Parameters. (continued)**

Contractual Specs	Design								
<p>Random vibration (cont):</p> <table> <tr> <td>Frequency (Hz)</td><td>PSD (<math>\text{g}^2/\text{Hz}</math>)</td></tr> <tr> <td>200-700</td><td>0.150</td></tr> <tr> <td>700-2000</td><td>-4 dB/octave</td></tr> <tr> <td>Composite</td><td>13.7 g rms</td></tr> </table> <p>Duration of 2 min along each of 3 orthogonal axes</p>	Frequency (Hz)	PSD ( $\text{g}^2/\text{Hz}$ )	200-700	0.150	700-2000	-4 dB/octave	Composite	13.7 g rms	
Frequency (Hz)	PSD ( $\text{g}^2/\text{Hz}$ )								
200-700	0.150								
700-2000	-4 dB/octave								
Composite	13.7 g rms								
<p>Sine survey:</p> <p>0.5 to 1.0 g</p> <p>15 to 100 Hz</p> <p>One sweep up and down in each axis at 2 octaves/min</p>	Designed to meet								
<p>Transient shock:</p> <p>25 g, 11 ms, half-sine pulse along each axis</p>	Designed to meet								
<p>Thermal vacuum:</p> <p><math>&lt;10^{-5}</math> Torr</p> <p>-24°C to +61°C</p> <p>12 h at the low and high temperature levels</p>	Designed to meet								
<p>Thermal cycling:</p> <p>Ambient pressure</p> <p>-24°C to +61°C</p> <p>&gt;8 cycles with 2 h dwell at low and high temperature, transitions at <math>\geq 3^\circ\text{C}/\text{min}</math></p>	Designed to meet								
<p>Burn-in:</p> <p>Ambient pressure</p> <p>-24°C to +61°C</p> <p>&gt;18 total cycles including those above</p>	Designed to meet								
<p>Depressurization/repressurization:</p> <p>Shuttle profile</p> <p>JSC 07700 Vol. XIV</p> <p>Attachment 1, rev. G</p>	Designed to meet								

### SECTION 3

#### ELECTROSTATIC ANALYZERS

The FMDS incorporates ESAs to measure the distribution of ion and electron energies which are incident on the spacecraft. The ESAs are important to the FMDS charging-detection function because they are the only instruments of those specified for FMDS that can detect the onset of eclipse charging. (The SPMs respond too slowly when the spacecraft is in darkness.) The data can be analyzed to determine the actual vehicle potential (i.e., frame potential relative to space potential) rather than the dielectric-surface potentials monitored by the SPMs. In addition to these important charging-detection attributes, the ESAs provide valuable scientific information.

The ESAs that are employed on the FMDS are configured with short-cylindrical section sensors. Instruments of this type have been used in physics experiments since the turn of the century, and similar devices have been flown on many spacecraft. The FMDS instrument incorporates 16 channels and fast sweep times in order to provide the rapid reaction time that is required in the FMDS mission.

The ESAs for the FMDS are being provided by Panametrics Inc. of Waltham, MA under subcontract. The design of this instrument has not changed during the past 12 months and last year's report<sup>1</sup> should be consulted for further details.

## SECTION 4

### SURFACE POTENTIAL MONITORS

Two Surface Potential Monitors (SPMs) are included as part of the FMDS to detect the charging of dielectric surfaces on the satellite. Since two different dielectric materials are to be used in flight, and since it is desirable to have them physically separated (to minimize their effect on each other), the best approach was to use two instruments, with the dielectric material being the only difference (see Figure 2-2).

#### 4.1 BASIC SPM DESIGN

One of the main factors in the design of the SPMs is the requirement of not altering the charge buildup of ions or electrons on the dielectric material due to the measurement. This dictates that some type of essentially infinite-impedance electric-field-sensing device be used.

Most electrostatic voltmeters that have sufficient accuracy and resolution use a field-sensing probe that is closed-loop controlled to the same potential as the surface being measured. In this way the field sensor need only detect a null. To use this approach in this application a "servo-amplifier" with an output of  $\pm 20$  kV would be required; this is not practical within the weight and power limitations for this instrument. We have chosen, therefore, to use the approach that was adopted by NASA's Lewis Research Center for their surface-voltage sensor (SVS).<sup>2</sup> NASA's approach retains most of the advantages of a feedback sensing system, yet does not require high voltage. This system uses a combination of electrodes that attenuate the field produced by the sensing surface and allows it to be nulled with a low-voltage ( $< \pm 10$ -V) feedback signal (see Reference 1 for details).

#### 4.2 SPM DESIGN CONSIDERATIONS

The flight design of the SPM is shown in Figure 4-1 where the input electrode is supported by an annular insulating ring. This allows the dielectric sample to extend past the input electrode onto the annular insulating ring, thereby shielding the electrode from any particles or plasma that are in the immediate vicinity. The input electrode with the dielectric material on its surface is insulated from the rest of the instrument by the annular insulating ring. The electrostatic voltmeter measures the potential of the input electrode; however, no direct electrical connection is made to it. The potential of the front surface of the dielectric is transferred to the input electrode by capacitive coupling. Therefore, if the input electrode is to closely track the dielectric front surface, the capacitance from the input electrode to ground must be much smaller than the capacitance between the dielectric front surface and the input electrode.

A possible problem with the SPM is that the input electrode could gather some charge not related to the potential of the dielectric front surface. This charge would then introduce a zero offset into the SPM. The breadboard design called for a shorting relay and software routine that would connect the input electrode to ground when the SPM was in full sunlight. Under full sunlight conditions the dielectric front surface should be within 100 V of ground and therefore, the SPM would be zeroed to within 100 V. This scheme required that the spacecraft periodically rotate the SPMs into full sunlight. This requirement and the need for a small lightweight 20-kV relay turned out to be a significant engineering problem.

The flight design calls for deleting the relay and using a 2-hour time constant R-C network to discharge the input electrode. A 2-hour time constant network requires approximately  $2.4 \times 10^{13}$  ohms from the input electrode to ground; this could conceivably be provided by the leakage of the annular insulating ring but a



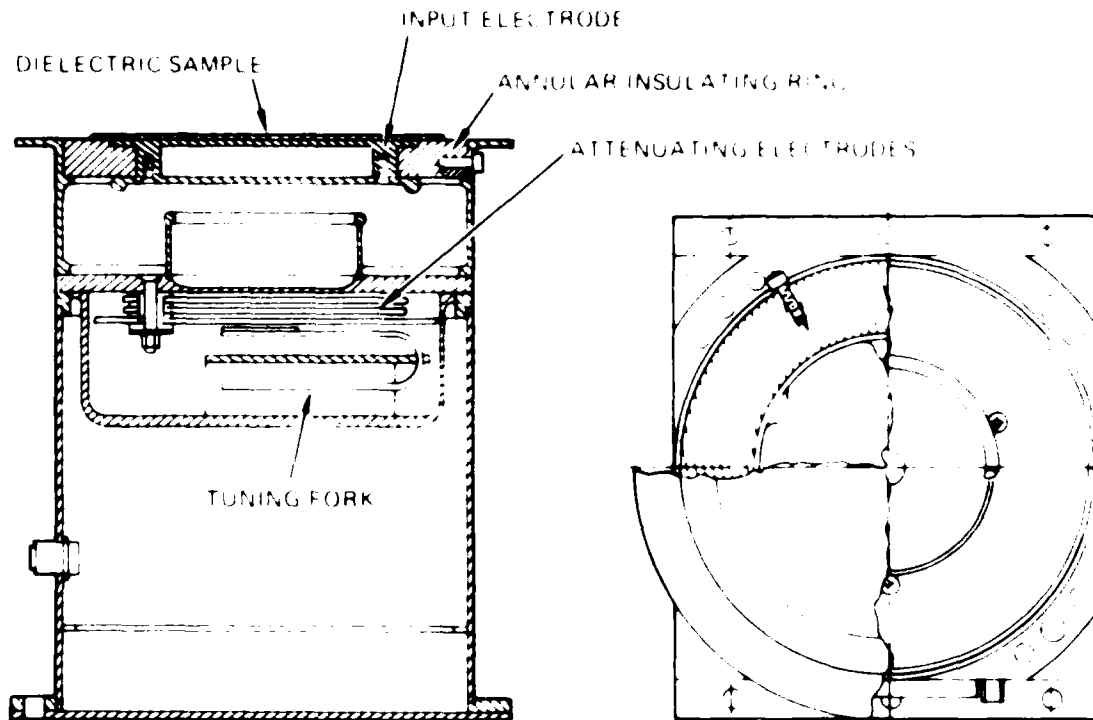


Figure 4-1 Flight package design for the SPM

bleed off resistor will be added. A normal operating scenario will be that differential charging exists which will immediately charge the front surface of the dielectric, and the input electrode will go to the same potential. The 2-hour time constant network will start to bleed the charge from the input electrode; however, differential charging normally occurs in minutes and if it is of any significant level, the plasma source will be turned ON. The plasma source will immediately remove the charge from the front surface of the dielectric and return it to ground. The 2-hour time constant network will then reset the input electrode to ground. The problem with this approach is that very slow differential charging will not be detected by the SPMS.

We tried using Vespel for the annular insulating ring and tested it in a vacuum chamber under simulated operating conditions. Vespel demonstrated an acceptable initial time constant; however, the input electrode decayed toward a voltage level that was in the range of 25 to 90% of the voltage originally applied to the input electrode, the level depending on the length of time the voltage was applied before allowing the input electrode to start decaying. The input electrode appeared to decay with a much longer time constant ( $>$  factor 10) after the initial time constant. Fused silica and G-10 glass epoxy exhibited characteristics similar to the Vespel.

The decay characteristics of the input electrode are not fully understood at this time. Further tests are planned to resolve this question.

## SECTION 5

### TRANSIENT PULSE MONITOR

The Transient Pulse Monitor (TPM) is included as part of the FMDS to detect the onset of arcing on spacecraft surfaces. The main criterion for the selection of the TPM sensor design is the requirement to maximize the ability to discriminate between signals generated by arcing events and signals due to "legitimate" spacecraft circuit transients. A secondary consideration is the necessity to register arcs occurring anywhere on the spacecraft surface with a minimum number of sensing elements.

A review of the literature revealed that the main types of effects caused by arcing on a spacecraft are:

- (1) The arc causes "blow-off" of a cloud of electrons which rapidly disperses. This geometrical change causes a pulse of electrostatic field which can be detected by capacitive coupling to an electrometer plate. This electrostatic field can be detected, weakly perhaps, beyond the line-of sight.
- (2) The arc creates a plasma which radiates at high frequency. This causes a pulse of wide-band rf energy to appear, with its source in the plasma cloud and randomly polarized. This energy can be detected by antennas (horns, dipoles, monopoles, etc.); for the most part, the radiation can be sensed in line-of-sight only.
- (3) During the pre-arc stage, an increasing electrostatic potential appears (probably at the surface) of dielectric materials. The arc causes a substantial collapse of this potential, which can be detected by capacitive coupling to an electrometer plate. The width of the detected pulse is determined by the low frequency response of the detection equipment, rather than any characteristic of the arc signature itself. The collapse of the potential can be detected beyond the line-of-sight.
- (4) The arc causes replacement currents, which can be detected by current sensors, to flow in the conducting skin of the satellite.

Effect (4) has been employed on several satellites (e g SCATHA and Canadian Technology Satellite) as a means of detecting arcs. The major problem encountered with this technique is its inability to differentiate between arcs and legitimate spacecraft transients, particularly in real time. Therefore, it was not seriously considered for this application.

The remaining effects can be classified by the type of detector required. Effects (1) and (3) utilize an electrometer plate (E field antenna), which is broadband, while effect (2) requires an rf antenna, which is narrow band. The relative merits of these two detection methods are as follows:

- If only a single detector with a single antenna outside the Faraday cage of the spacecraft is used, the ability to discriminate correctly between arcs and transients appears to be equally limited for both detection methods.
- A single broadband antenna is more likely than a single rf antenna to pick up a detectable signal from an arcing event occurring at a location that is far below the horizon of the antenna, i.e., far from having a line-of-sight connection with it.
- Regardless of the detection method, the addition of a second antenna inside the spacecraft Faraday cage, in conjunction with a simple pulse-analysis circuit, offers a much increased probability of correct discrimination between arcs and transients by permitting a comparison between the signals received inside and outside of the Faraday cage.
- It is more likely for the signals received by two broadband antennas, rather than for those received by two rf antennas, that their amplitude ratios will characterize arcs and transients properly, irrespective of the location of the event relative to that of the antennas.
- Additional practical points in favor of the broadband approach are the ease of protection from destructive overloads due to arcs adjacent to the antenna, and the lower power consumption.

The TPM design for FMDS is based on the broadband detection approach utilizing a  $123 \text{ cm}^2$  E-field antenna outside of the spacecraft Faraday cage connected to a 250-Hz to 75-MHz broadband amplifier and pulse analysis circuitry, and a second  $123 \text{ cm}^2$  E field antenna with greatly simplified pulse analysis capabilities inside the Faraday cage. The detailed design is discussed in last years report.<sup>1</sup>

## SECTION 6

### CONTROLLER

The controller provides autonomous control of the FMDS relative to the remainder of the satellite and also ties the other units of the FMDS together. The "brain" of the Controller is a microprocessor which contains the algorithms necessary to interpret the data from the sensors and command the plasma source to turn ON when spacecraft charging is occurring. It then monitors the operation of the plasma source and maintains it in stable operation. The controller turns the plasma source OFF after a programmable time-out, when the emission current from the plasma source has been less than a threshold value for a specified period of time, and/or the ambient electron environment returns to a quiescent condition. The controller has the ability to accommodate certain instrumental faults and failures and to adjust instrument parameters. It is also the command and telemetry interface with the satellite.

The only change to the controller from last years report<sup>1</sup> is the redesign of the analog-to-digital converter (ADC) because of a part-procurement problem. National Semiconductor has stopped producing rad-hard CMOS and therefore the 54C905 successive-approximation-register (SAR) we were planning to use is no longer available in the rad-hard version (except at an exorbitant cost - \$25,000 to \$30,000 for the six parts we need). Other SAR's are available, however, they are not CMOS and would consume 300 to 500 mW compared to 2 mW for the 54C905.

For these reasons, it was decided to switch from the SAR type of ADC to a counting type of ADC. The only disadvantage of the counting ADC is the conversion time. The SAR ADC had a total conversion time (from the software viewpoint) of approximately 75  $\mu$ s (independent of the analog voltage being converted). The counting ADC will have a total conversion time of approximately 45 to 300  $\mu$ s depending on the analog voltage being converted.

Therefore, the counting ADC will require a maximum of 4 times as long (9.6 ms) to convert all 32 analog channels as compared to the SAR ADC. The 9.6 ms represents 0.24% of the total software cycle time and is not a factor in the overall system. Figure 6-1 shows the SAR ADC and Figure 6-2 shows the new counting ADC. The major difference is that the 54C905 in Figure 6-1 has been replaced by two CD40161s and a CD4011 in Figure 6-2. This change has a minimal impact on the printed wiring board layout. (NOTE: This same change will be incorporated into the TPM).

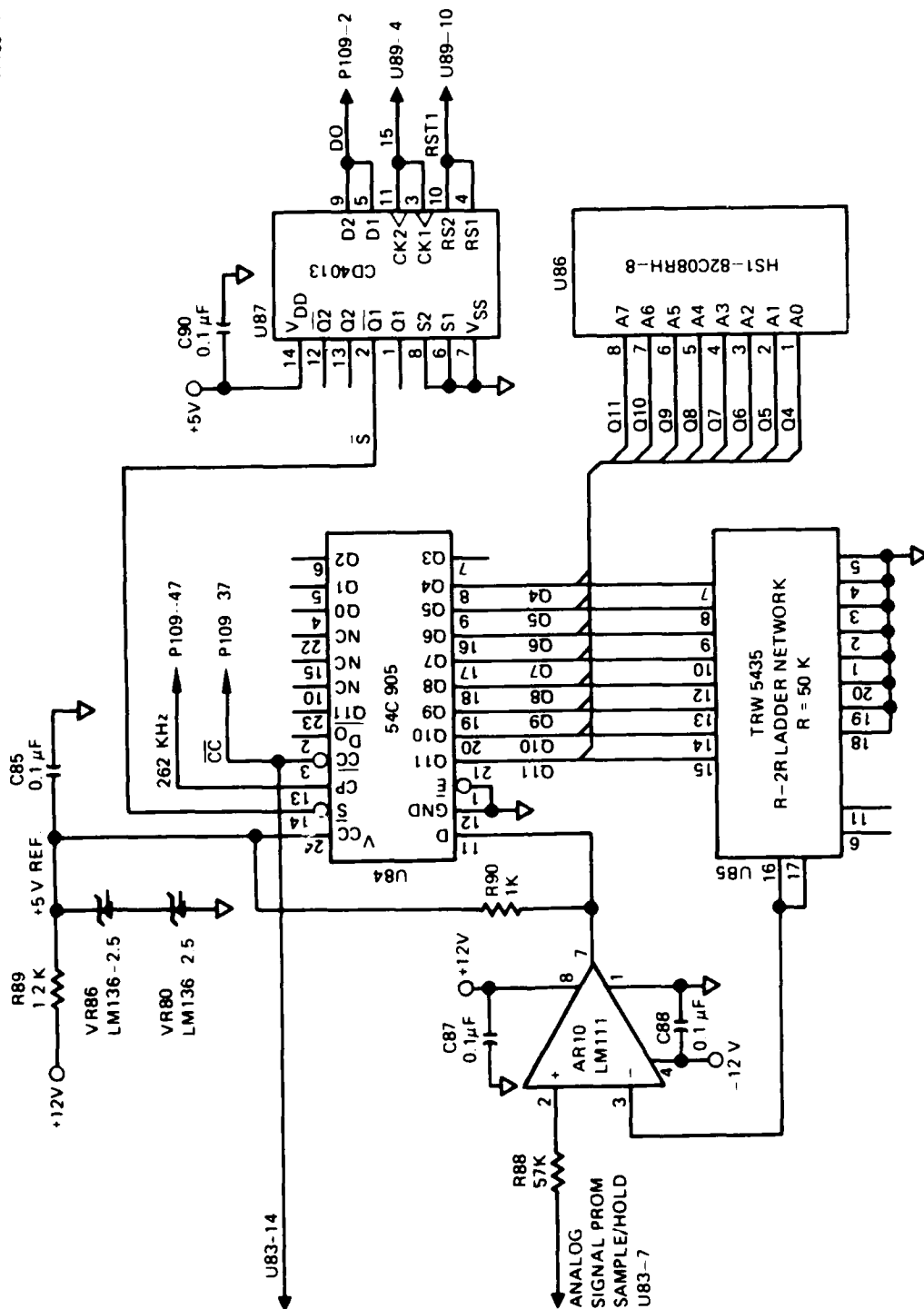


Figure 6-1. Successive approximation register A/D converter originally planned for FMDS.



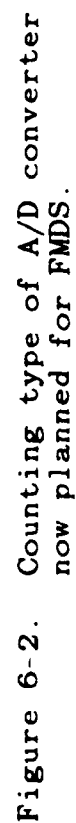


Figure 6-2. Counting type of A/D converter now planned for FMDS.

## SECTION 7

### PLASMA SOURCE

The FMDS plasma source consists of three subsystems: the plasma generator, the power electronics required to operate and control the plasma generator, and the expellant storage and control assembly. The plasma generator has been developed under a Hughes IR&D project and this technology has been provided to the FMDS program for the flight plasma generator design. The following sections discuss the design of and the latest test results on the plasma generator.

#### 7.1 PLASMA GENERATOR DESIGN

The plasma generator is regarded as the major element of the system, since its design and operating characteristics determine the requirements for the other two elements (power supplies and feed system). The plasma generator has the general characteristics shown in Table 7-1.

The plasma generator (Figure 7-1) is a compact arrangement of a hollow-cathode, keeper and anode electrodes, a magnetic structure, and a ground shield. Xenon gas flowing through the plasma generator is ionized by bombardment with electrons released from a low-work-function surface within the hollow cathode. The ionized gas flows out of the plasma generator, providing a medium density ( $\sim 10^{16}/\text{cm}^3$ ), inert-gas plasma to neutralize differential charge buildup between various surfaces of the spacecraft and also to form an electrically conducting "bridge" between the spacecraft and the natural space plasma.

A less than 1-s turn-ON time of the plasma generator is achieved by gas-burst ignition. Approximately 1000 V is applied between the keeper and the cathode and then a burst of high-pressure gas (few hundred Torr) is admitted to the cathode. The

Table 7-1. SPACECLAMP Plasma Generator Characteristics

14881-22R1

PARAMETER	VALUE	UNIT
EXPELLANT FLOW RATE	< 40	mA EQUIV
DISCHARGE VOLTAGE	< 40	V
DISCHARGE CURRENT	< 250	mA
KEEPER VOLTAGE	< 25	V
KEEPER CURRENT	< 400	mA
TOTAL POWER (RUN)	< 10	W
TOTAL POWER (ONE-TIME-ONLY CONDITIONING)	20	W
IGNITION TIME	< 1	S
EXPECTED LIFETIME	> 1200	HOURS
EXPECTED RESTART CAPABILITY	> 1000	STARTS
ION-EMISSION CURRENT (MAX)	> 1	mA

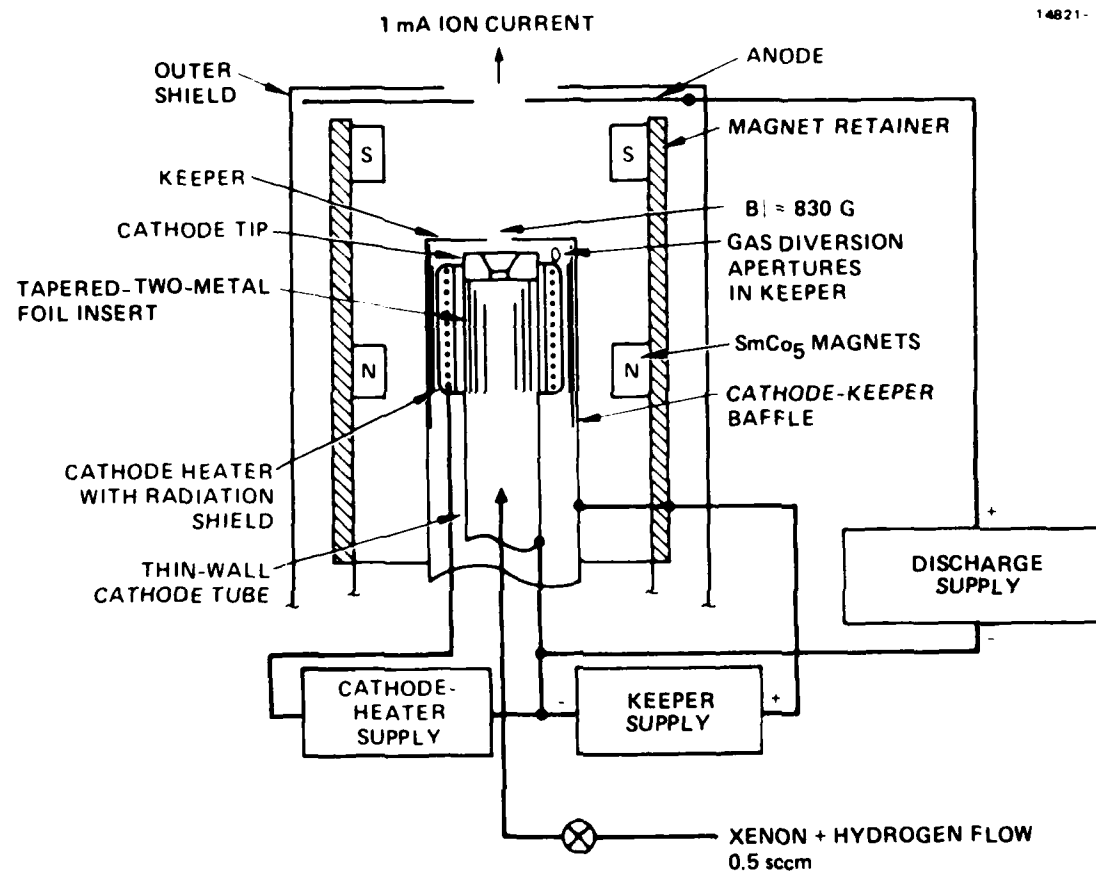


Figure 7-1. Simple schematic of the plasma generator.

keeper voltage falls almost immediately ( $<1$  ms) to  $<20$  V. We believe that the ignition process consists of the formation of an arc which runs on a small spot on the insert until the insert temperature is raised to the point of thermionic emission. At this point, cathode operation undergoes a rapid transition to a low-voltage hollow-cathode mode. The total energy input during the high voltage portion of the ignition transient is about 0.25 J, which is nondestructive to the the insert. The gas pressure and flow settle out to the nominal 0.5 sccm condition in approximately 120 s.

The rolled-foil insert consists of 0.013-mm (0.5-mil) thick rhenium foil with a sputter deposited linear platinum grid deposited on one side. A Hughes proprietary emissive mix is sprayed on both sides of the foil to provide a low work function medium for electron emission. The rhenium foil is then rolled into a cylindrical structure for insertion into the cathode.

The flight design of the plasma generator is shown in Figure 7-2. It is designed as a hermetically sealed unit so that it can be evacuated (through the remove-before-launch cap) and operated during ground testing and spacecraft integration. The cathode, keeper, and anode are all electrically isolated from the outer shell so that the return current from the spacecraft can be measured.

## 7.2 TEST RESULTS

During the past year under our IR&D, we completed and surpassed the goals of a cyclic lifetest of a breadboard plasma generator. The test was designed to demonstrate plasma source lifetime in excess of 1,200 hours and 1,000 ignitions to satisfy mission goals in applications such as FMDS. It had demonstrated 1,562 hours of operation and 1,582 cold gas burst starts when we voluntarily terminated the test to permit detailed inspection of

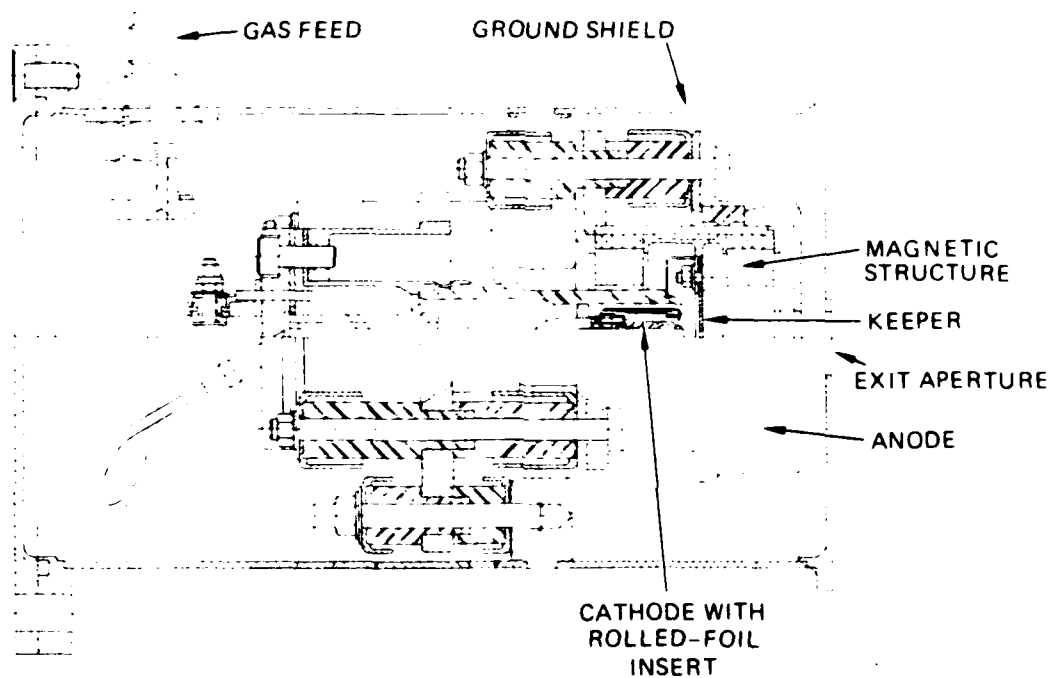


Figure 7-2. Cross section of the flight plasma generator.

the plasma source. The cathode and cathode insert were both in excellent condition, indicating that we had not yet reached the end of lifetime for these critical plasma source components.

This plasma generator is unique compared to other hollow cathode plasma generators because of its ability to be started in less than one second from a cold cathode condition. Hollow cathodes have traditionally required several minutes to start; the several minutes being used to raise the cathode to emissive temperatures via a resistive heater.

The significant aspects of this lifetest relative to previous tests are:

- (1) Use of a 90% xenon and 10% hydrogen gas mixture (as opposed to pure xenon) to ameliorate what we believe to be water vapor deconditioning of the cathode insert.
- (2) The cathode tube is made of a molybdenum-rhenium alloy, chosen for its resistance to chemical attack from the emissive mix and embrittlement by hydrogen.
- (3) The peak keeper current from the 1-kV igniter supply has been reduced from 1 A to 0.4 A.
- (4) An inductor has been added to the output of the keeper supply to accommodate short duration instantaneous voltage transients required by the plasma generator during the first 20 s after ignition.

As a result of this life test, several observations can be made.

- (1) The 90/10 xenon/hydrogen gas mixture improves the gas-burst-ignition characteristics while not affecting other operating parameters.
- (2) A minimum ON time of 1 hour improves the gas-burst-ignition characteristics of subsequent cycles.
- (3) Periodic reconditioning of the plasma generator is necessary for reliable ignitions. We recommend after every 100 ignitions since the vast majority of ignition

faults during this lifetest occurred after 100 cycles since the last reconditioning. Reconditioning consists of applying 20 W of tip heat for 1 hour and then operating the plasma generator for 1 hour without tip heat.

- (4) Steady-state performance (after being ON for approximately 120 s) is very reliable.

Throughout the course of the lifetest, we utilized a variety of computer-controlled operating modes. The ON times ranged from 2 minutes to 2 hours, and the OFF times from 1 to 59 minutes. The computer system was capable of performing an immediate restart of the plasma generator if it did not start successfully. After three successive failures, the computer shut the test down and waited for operator-controlled reconditioning to be performed. Reconditioning, which refreshes the layer of work-function-reducing emissive mix on the cathode insert surfaces, returns the ignition characteristics to a satisfactory condition, and was performed several times during the lifetest.

The ion-emission characteristics of the plasma source are shown in Figure 7-3 for various keeper and discharge current setpoints. The ion-emission current is relatively insensitive to keeper current and is mainly a function of discharge current. The keeper and discharge voltages as a function of expellant flowrate are shown in Figure 7-4 (keeper current = 255 mA, discharge current = 202 mA). The voltages start to rise rapidly below 0.5 sccm which is the nominal operating point and a good compromise between input power and expellant consumption.

The keeper current and voltage (on a fast time scale) are shown in Figure 7-5 during gas-burst ignition. On this time scale, both are well behaved and quickly settle out. However, Figure 7-6 shows that the plasma generator is quite noisy and its operating parameters varying during the first two minutes of operation. This is believed to be associated with the cathode



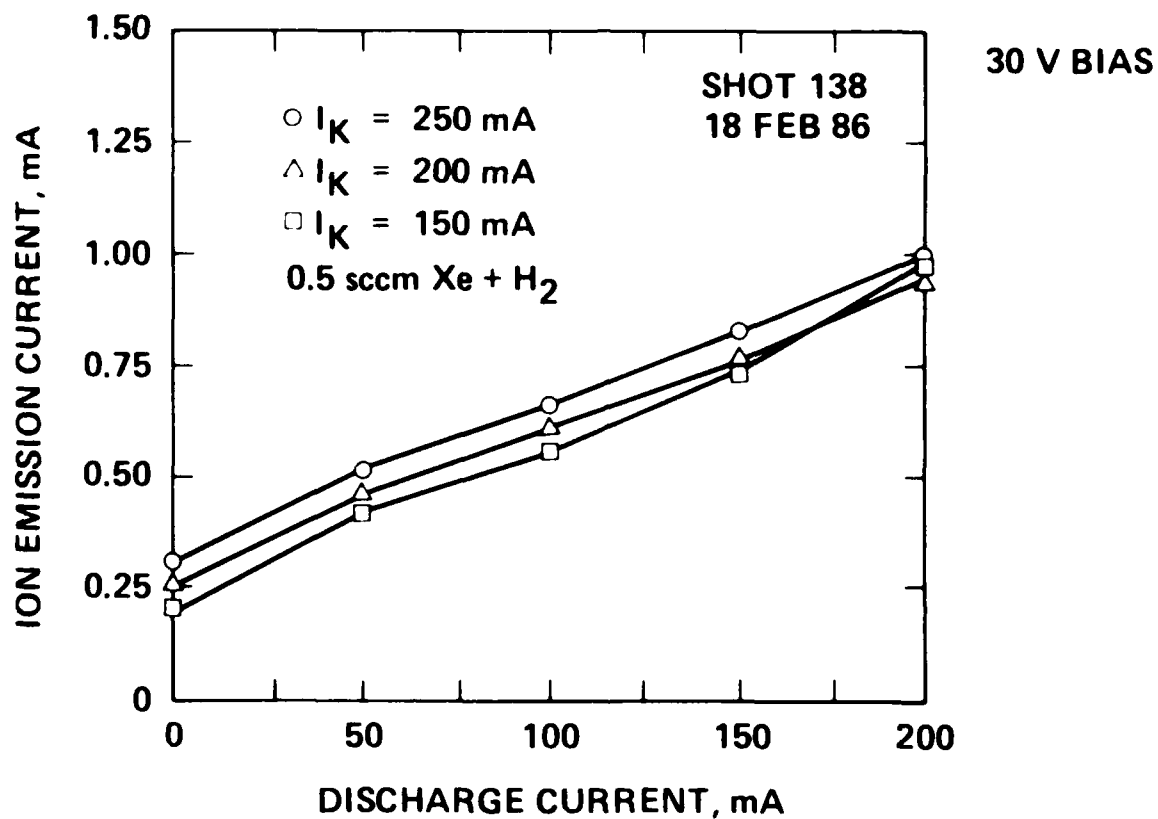


Figure 7-3. Ion emission current characteristics of the plasma generator for various keeper and discharge current setpoints.

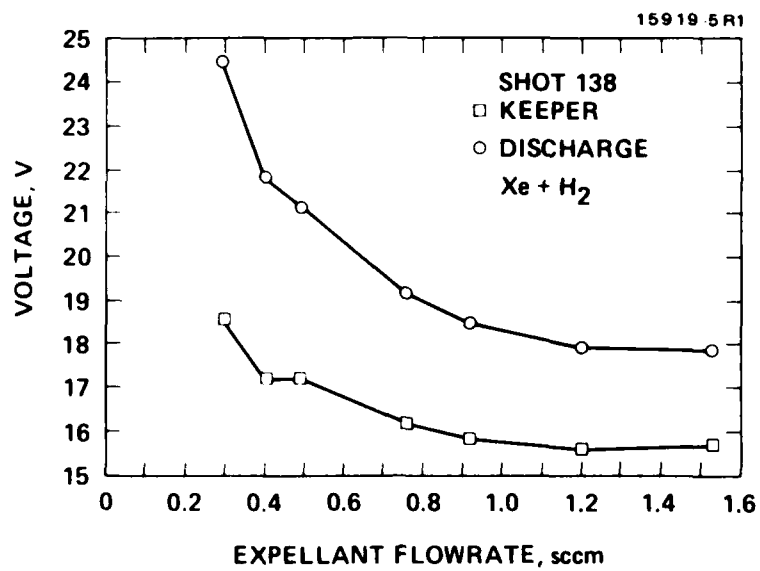
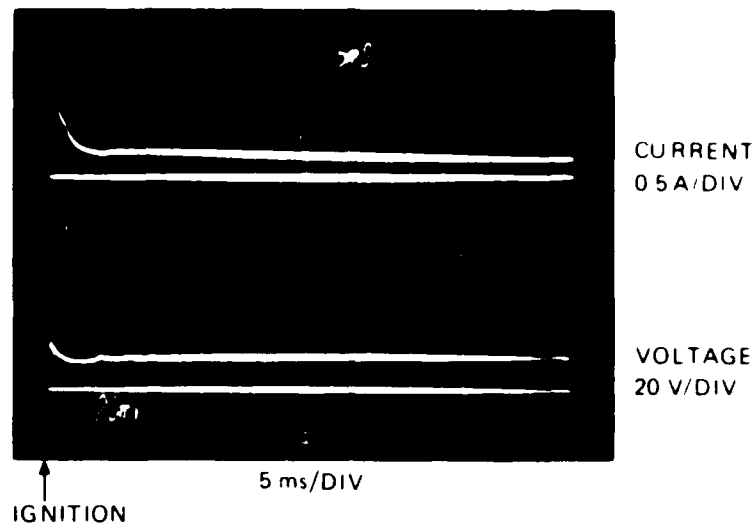


Figure 7-4. Keeper and discharge voltages as a function of expellant flow rate.

## SHOT 66



## SHOT 143

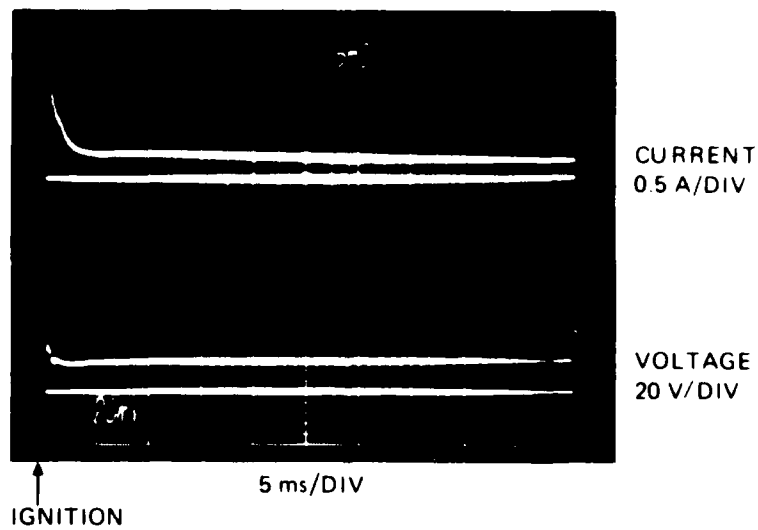


Figure 7-5. Keeper current and voltage during gas burst ignition.

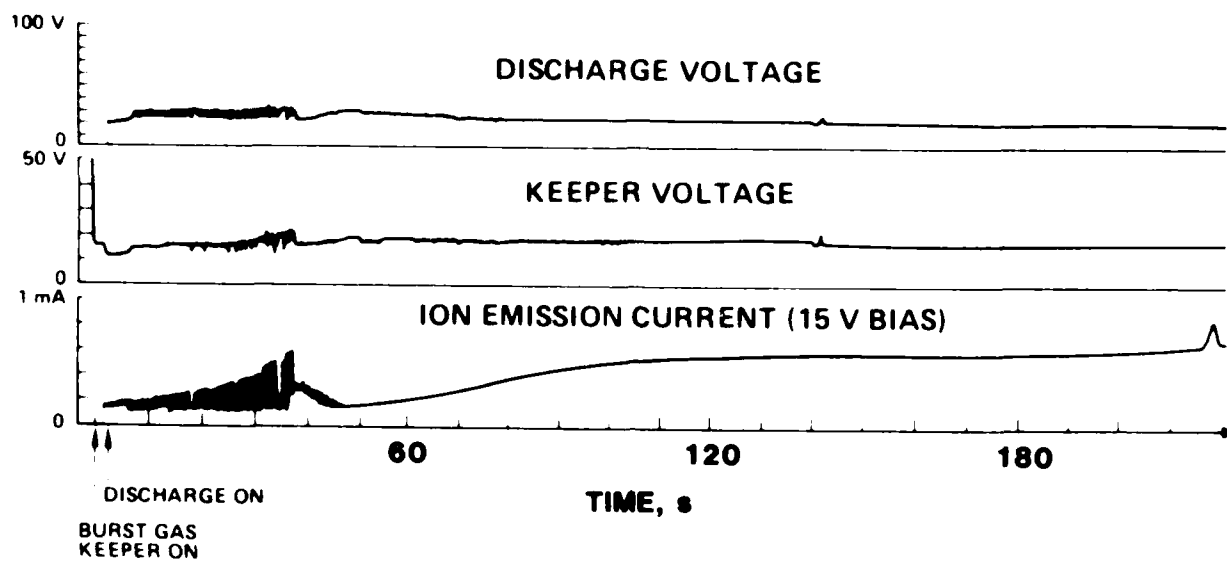


Figure 7-6. Plasma source voltages and ion emission during the first few minutes after starting.

coming up to operating temperature and the flowrate decreasing to 0.5 sccm (after the gas burst for ignition).

FMDS is ultimately intended for use on operational spacecraft where hydrogen in the expellant will not be a problem. However, the use of hydrogen in the expellant could be a problem if FMDS is used on some scientific spacecraft. The plasma generator will expel protons and protons are the dominant natural species in space. If hydrogen were a problem, then deuterium might be acceptable, depending on the scientific measurements being made. Deuterium is expected to have the same ameliorating effects on the plasma generator as hydrogen.

Hydrogen is also always a concern from the safety standpoint. The FMDS expellant tank will contain 10 standard liters of  $H_2$  and explosive mixtures in air or oxygen require  $H_2$  concentrations greater than 4%. Therefore if all 10 standard liters were immediately dumped into a volume greater than 250 liters ( $9 \text{ ft}^3$  or a cube 2.1 ft on a side), the mixture would not be explosive. For this reason, we believe the quantity of hydrogen carried by FMDS is not a safety hazard.

### 7.3 CONTAMINATION MEASUREMENTS

The possibility of contaminants emanating from a plasma generator is always a concern to spacecraft designers, especially where optical and thermal control surfaces are involved. Therefore, during the lifetest of the breadboard plasma generator, we installed three glass "witness" slides within the vacuum chamber to measure the deposition of any contaminating substances that might emanate from the plasma generator.

The slides were placed in the positions shown in Figure 7-7. Slide #3 was directly below the exit aperture of the plasma generator and slide #4 was approximately 17 cm further downstream. Both slides were mounted on a perforated steel mesh

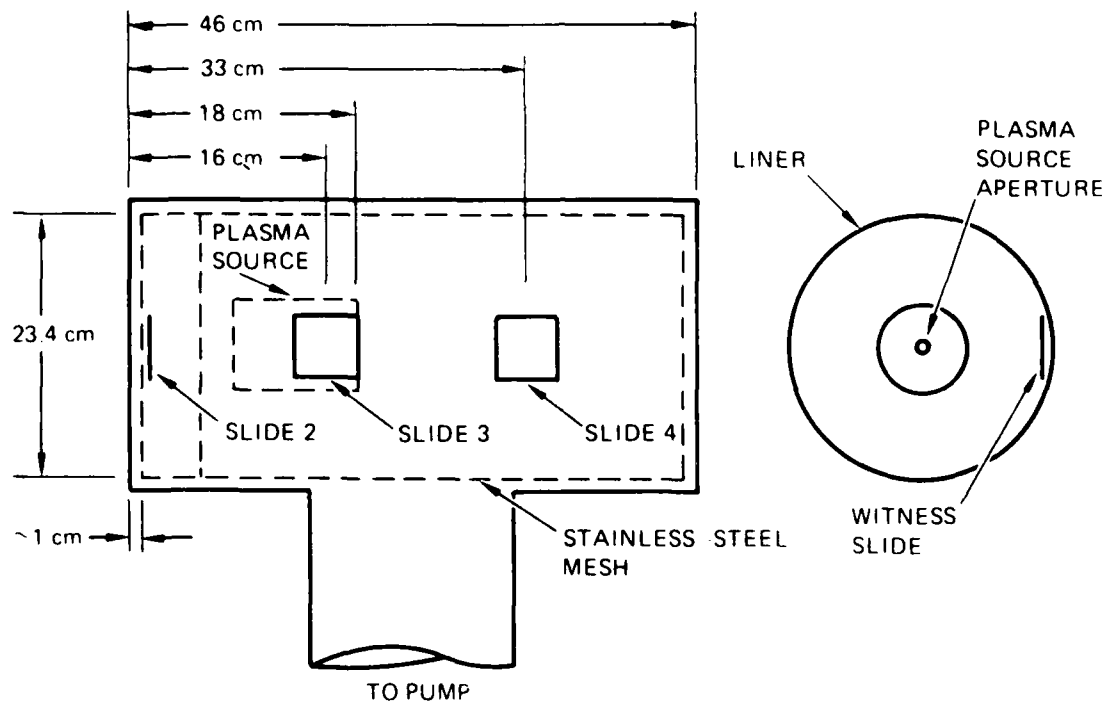


Figure 7-7. Positions of the contamination "witness" slides during the plasma generator lifetest.

vacuum-chamber liner (diameter = 23.4 cm). Slides #1 and #2 were control slides, with #2 being placed within the vacuum chamber but upstream of the plasma generator and isolated from the emitted plasma by a perforated mesh. Slide #1 was never placed in the vacuum chamber.

After the lifetest, we found that slide #3 had become coated with a brownish material while slides #2 and #4 still appeared clear. Light transmission analysis of all four slides indicated that slides #1, #2, and #4 all had similar characteristics, while slide #3 showed transmission loss compared to the other three slides. This transmission loss as a function of wavelength is shown in Figure 7-8. We used ESCA (electron spectroscopy for chemical analysis) to measure the relative amounts of any surface-deposited elements on slides #1, #3, and #4. No contaminants were identified on slides #1 and #4 while slide #3 was found to have carbon and sodium on it. We believe that this contamination is due to vacuum-pump oil that backstreamed onto the slide and subsequently decomposed under bombardment by plasma ions and electrons.

The types of contaminants that might possibly be emitted from the plasma generator are barium, strontium, calcium, platinum, rhenium, molybdenum, iron, samarium, cobalt, stainless-steel, tantalum and tungsten. None of these were found on the witness slides.

Another possible concern to a spacecraft is the condensation of the xenon expellant on cryo-temperature surfaces. Neutral xenon gas released from the plasma generator will condense and freeze (xenon has a 161°K freezing point) on cold (100°K) optical surfaces, potentially forming a thin xenon-ice coating that could degrade the optical properties of the cold optical elements. We present very simple calculations below which indicate that no buildup of condensing xenon will occur at the 100°K optical-

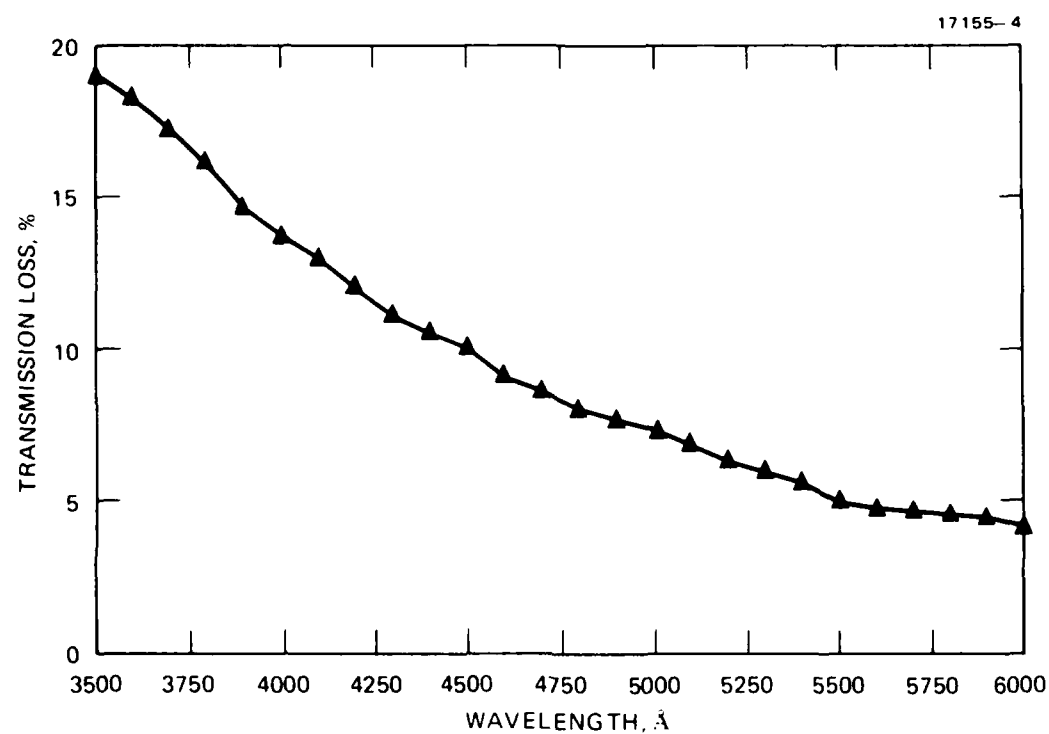


Figure 7-8. Optical transmission loss of contamination "witness" slide 3.



surface temperature and that only a small fraction of a monolayer of xenon surface coverage can be expected.

The rate of buildup of xenon on a cold surface can be computed by evaluating the xenon arrival rate (due to xenon diffusion from the plasma generator) and loss rate (due to xenon evaporation at 100°K from the cold optical surface).

The flux of neutral xenon arriving on an exposed surface is

$$f_{\text{arriving}} = n_0 \langle v_0 \rangle / 4,$$

where  $n_0 = \sim 10^{14} \text{ m}^{-3}$  is the assumed neutral-xenon density, and  $\langle v_0 \rangle = 194 \text{ m/s}$  is the mean xenon-atom velocity (assuming a 300°K temperature). These approximate numbers give an arriving flux of about

$$f_{\text{arriving}} = 5 \times 10^{15} \text{ m}^{-2} \text{ s}^{-1}.$$

The loss flux can be estimated by assuming that there is a thin xenon-vapor layer above the cold surface that is in equilibrium with the adsorbed xenon immediately below it. This layer will have a pressure equal to the vapor pressure of xenon at 100°K: i.e., 100 Pa. This pressure corresponds to a gas density near the surface of

$$n_s = P/kT_s = 10^{23} \text{ m}^{-3},$$

giving a flux of leaving xenon atoms of

$$f_{\text{leaving}} = n_s \langle v_s \rangle / 4 = 3 \times 10^{24} \text{ m}^{-2} \text{ s}^{-1}.$$

These simple calculations predict that if there were a surface layer of adsorbed xenon, it would desorb approximately  $10^9$  times faster than it could be replenished from ambient xenon. This calculation confirms what intuition suggests: unless the pressure of xenon gas that reaches cryogenic surfaces exceeds the 100-Pa vapor pressure of xenon at 100°K, no frozen-xenon buildup will occur. Xenon pressures this high exist only inside the plasma generator itself and only for a few seconds during gas-burst ignition.

While the foregoing calculations show that no macroscopic xenon-ice buildup can be expected, a small fraction of a monolayer of xenon will form on exposed surfaces, due to the fact that arriving atoms spend a finite time on the surface before they are evaporated off. The equilibrium surface coverage increases with incident xenon flux, decreases with temperature, and varies somewhat with the composition of the optical surface. In a typical result,<sup>3</sup> investigators found 0.08 monolayers of xenon on a Pd substrate at 100°K: however, their incident xenon-atom flux was  $f_{\text{arriving}} = 3 \times 10^{17} \text{ m}^{-2} \text{ s}^{-1}$ , which is greater than our expected flux by a factor of ~40. It requires very sophisticated experiments to detect even one monolayer; therefore, the buildup of xenon from the plasma generator should not affect the operation of any optical surfaces or sensors.

#### 7.4 MAGNETIC FIELD MEASUREMENTS

One of the specifications for the FMDS is that magnetic fields should be less than 100 nT at 1 m in any direction from the unit. Since the plasma generator contains permanent magnets, this specification is of primary concern. Measurements made on the unshielded flight magnetic field structure (using flight hardware) gave readings of 150 to 200 nT at 1 meter. The magnetic field structure is housed in a 3.25-inch-diameter by 5.5-inch-high cylinder that is closed on each end (except for the 0.5-inch-diameter exit aperture on the downstream end). Various methods of magnetically shielding this cylinder using Netic and/or Conetic materials were investigated and rejected because of fabrication problems. Fabricating the cylinder and downstream end plate from soft steel works as well as the special materials and is easy to fabricate. The final enclosure design is shown in Figure 7-2 and is expected to reduce the magnetic field to less than 50 nT at 1 meter.

## SECTION 8

### SYSTEM THERMAL ANALYSIS

The following sections summarize the results of the FMDS thermal analysis study from its inception in 1983 until its completion in September 1986. Figures and Tables are included which show predicted system temperatures under various conditions.

In addition to the development of an FMDS thermal model, certain key modules were analyzed. Steady state analyses of the TPM Threshold Detector, Master Microprocessor, and Plasma Generator Electronics (Shelf 2) Assemblies were performed. The purpose of these module analyses was to predict component operating temperatures and compare the results with the maximum acceptable component derated temperatures per Hughes S&CG document PA201. The CINDA thermal models used to calculate these temperatures are also included.

#### 8.1 ANALYSIS INPUTS

This section contains the physical and thermal configurations assumed for the thermal analyses.

##### 8.1.1 Physical Design

The FMDS system components mounted on the honeycomb mounting plate are shown in Figure 8-1. With the exception of the plasma generator, the system is covered with an aluminum enclosure. The enclosure sides are blanketed with Multi Layer Insulation (MLI) while the top is covered with quartz radiator and/or MLI. The normalized radiator area,  $A_R$ , is a key parameter in the presentation of the results to follow. The primary system components in Figure 8-1 are:

- Plasma Generator
- Plasma Generator Electronics
- Electrostatic Analyzer (ESA)
- Transient Pulse Monitor (TPM)
- Surface Potential Monitors (SPMs)
- Controller.

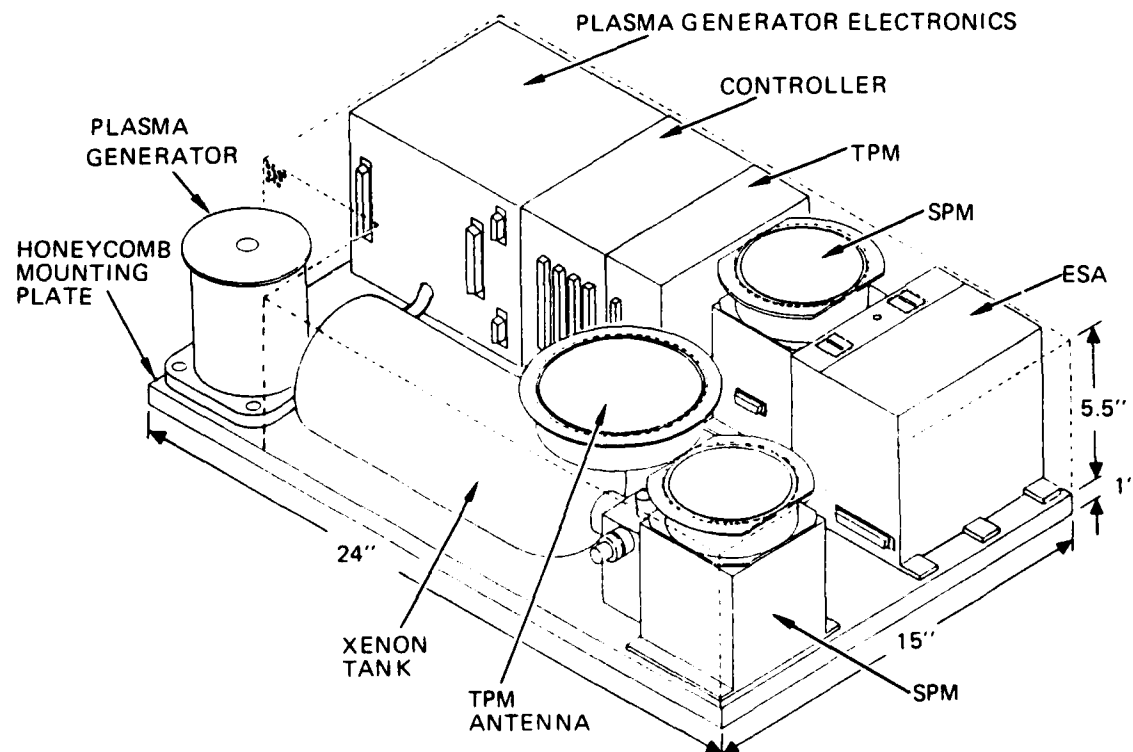


Figure 8-1. Flight Model Discharge System (FMDS).

The mounting position of the FMDS must be on an external surface of the satellite so that the ESA, TPM, SPMs, and Plasma Generator will have a view of the natural space environment. One such mounting position is shown in Figure 8-2.

The TPM Threshold Detector and Master Microprocessor Assemblies consist of a Multiwire board<sup>4</sup> mounted at the top and bottom to right angle brackets. A cross section of a typical Multiwire board is shown in Figure 8-3. A polyimide core 0.030 in. thick is coated on both sides with 2 ounce copper layers which serve as power and ground planes. A typical ground plane with cutouts for component and via holes is shown in Figure 8-4. Each layer of copper is covered with 0.006 in. of prepreg (adhesive layer) and glass epoxy which forms the outer surface of the board. A Multiwire board provides the conductive interconnections between electrical components through the use of insulated #34 AWG magnet wire embedded in the surface layer of the board.

The components in the Source Electronics Assembly are mounted on a 0.050 in. thick aluminum mounting plate which is 5.9 by 5.4 in.

### 8.1.2 Thermal Configuration

Figure 8-5 shows a simplified thermal model of the FMDS with boundary conditions at the satellite/FMDS interface as well as the space/FMDS and satellite-structure/FMDS interfaces which interact radiatively with the system. The top of the aluminum enclosure is tightly coupled to space when it is entirely covered with radiator.

The relationship between system-level and board-level analysis is shown schematically in Figure 8-6. The electronics boxes which are conductively connected to themselves, the top of the enclosure, and the honeycomb mounting plate are also radiatively connected to their interior surroundings. The latter point is true for all system components within the enclosure.

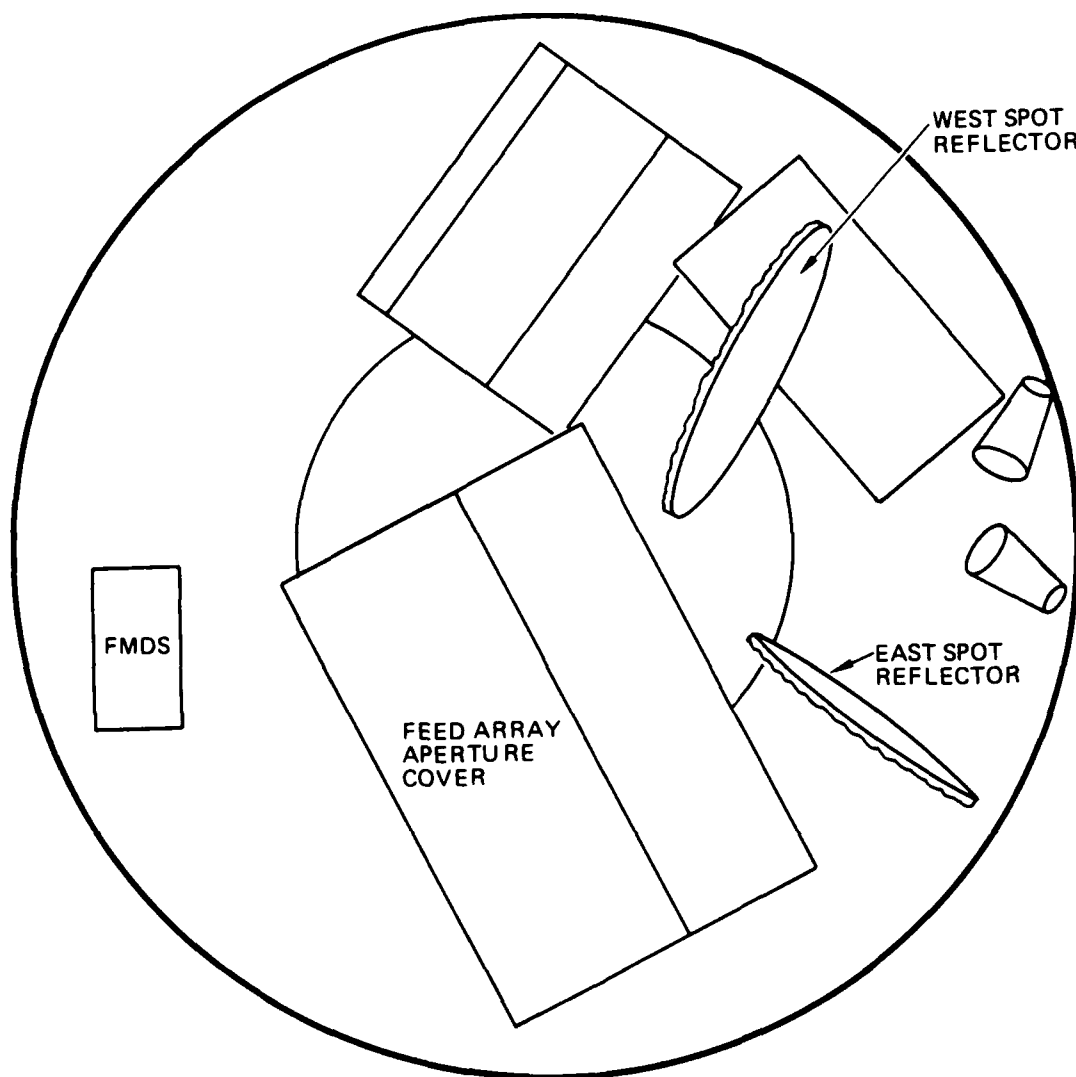


Figure 8-2. FMDS mounted near the antenna farm of a spin stabilized communications satellite.

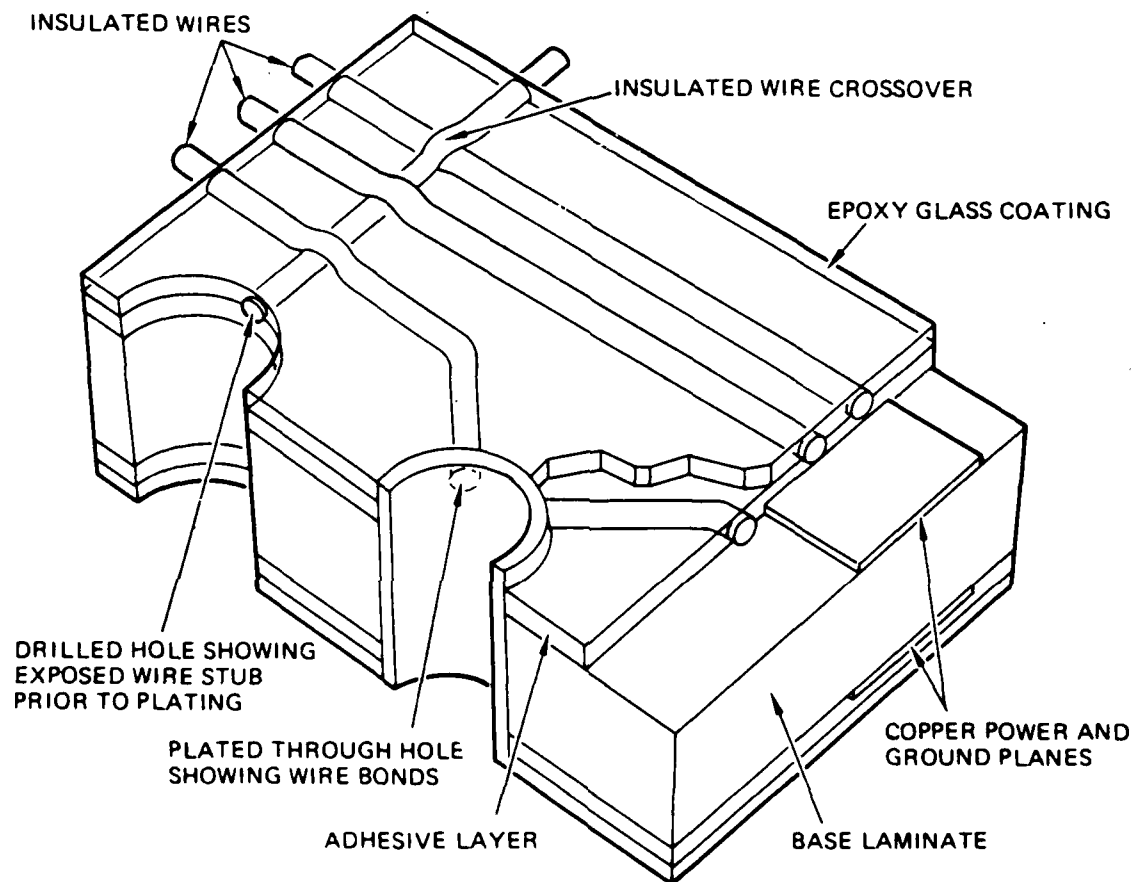


Figure 8-3. Cross section of a multiwire board.

16980-4

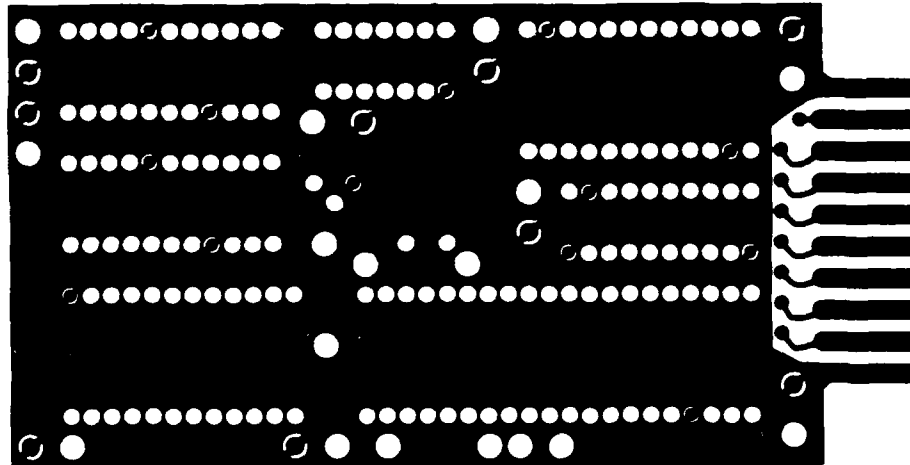


Figure 8-4. Typical multiwire board ground plane.



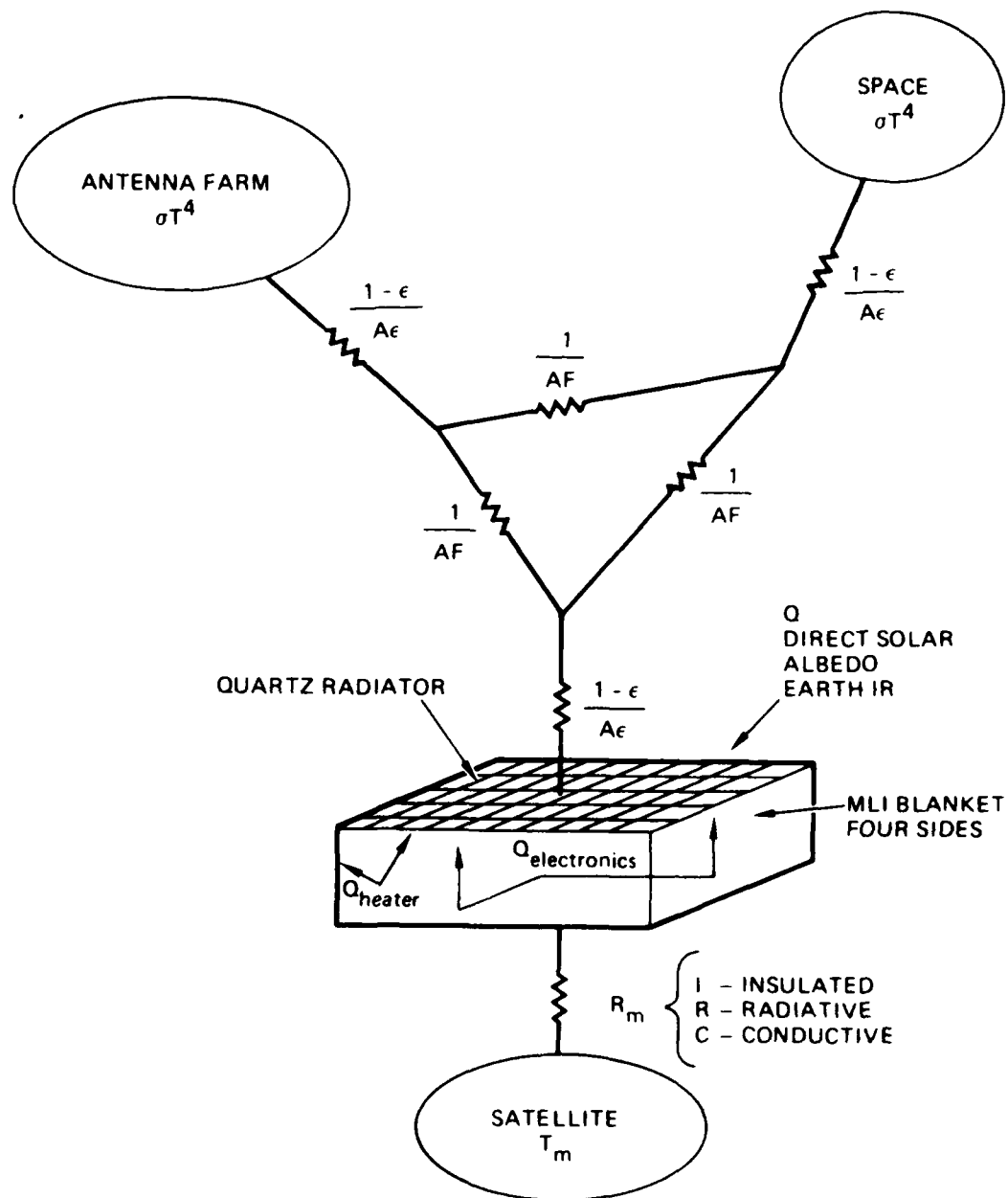


Figure 8 5. Simplified thermal model of the FMDS.

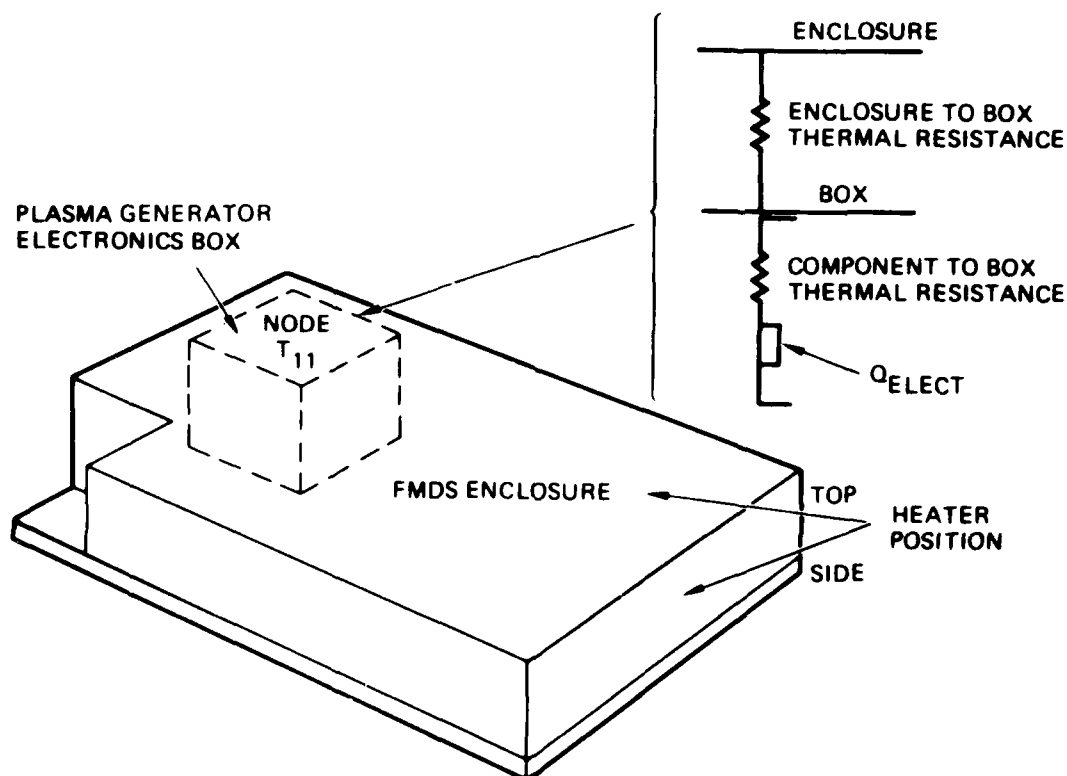


Figure 8.6. Typical enclosure/electronics-box/component thermal interface.

The Master Microprocessor and TPM Threshold Detector Assemblies are shown in Figures 8-7 and 8-8 respectively. Multiwire boards are used for both assemblies, and details of the different board layers are shown below. These boards are mounted by front surface right angle aluminum brackets 0.050 in. thick. It is assumed that all of the component-generated heat must flow through the board and exit at one of the right angle brackets. The two copper layers of the board provide most of the lateral heat path.

BOARD LAYER	MATERIAL	THICKNESS(inches)
1	epoxy	0.006
2	prepreg	0.006
3	copper	0.0028
4	polyimide	0.030
5	copper	0.0028
6	prepreg	0.006
7	epoxy	0.006
TOTAL		<u>0.0596</u>

The Plasma Generator Electronics (Shelf 2) Assembly (shown in Figure 8-9) is constructed around a 0.050 in. thick aluminum plate with the heat dissipating components bonded and/or stud-mounted to the plate. Interconnections between electrical components are hard wired with insulated via holes providing passage through the aluminum plate. Two components are mounted on transformer T1-CH and for these the mounting temperature is taken to be the transformer case temperature.

## 8.2 OPERATING CONDITIONS

A power dissipation map of the FMDS system is shown in Figure 8-10. Some minor changes to this map have occurred; however, this map is the baseline for the thermal analysis. The system has two basic modes of operation that are considered. The first, the "operating" mode, corresponds to operation of the plasma source and has the maximum dissipation (25.5 W). The second mode is the "monitoring" mode during which time the plasma source and its electronics are off and therefore not dissipating any power. The system dissipation for this mode is 10.5 W.

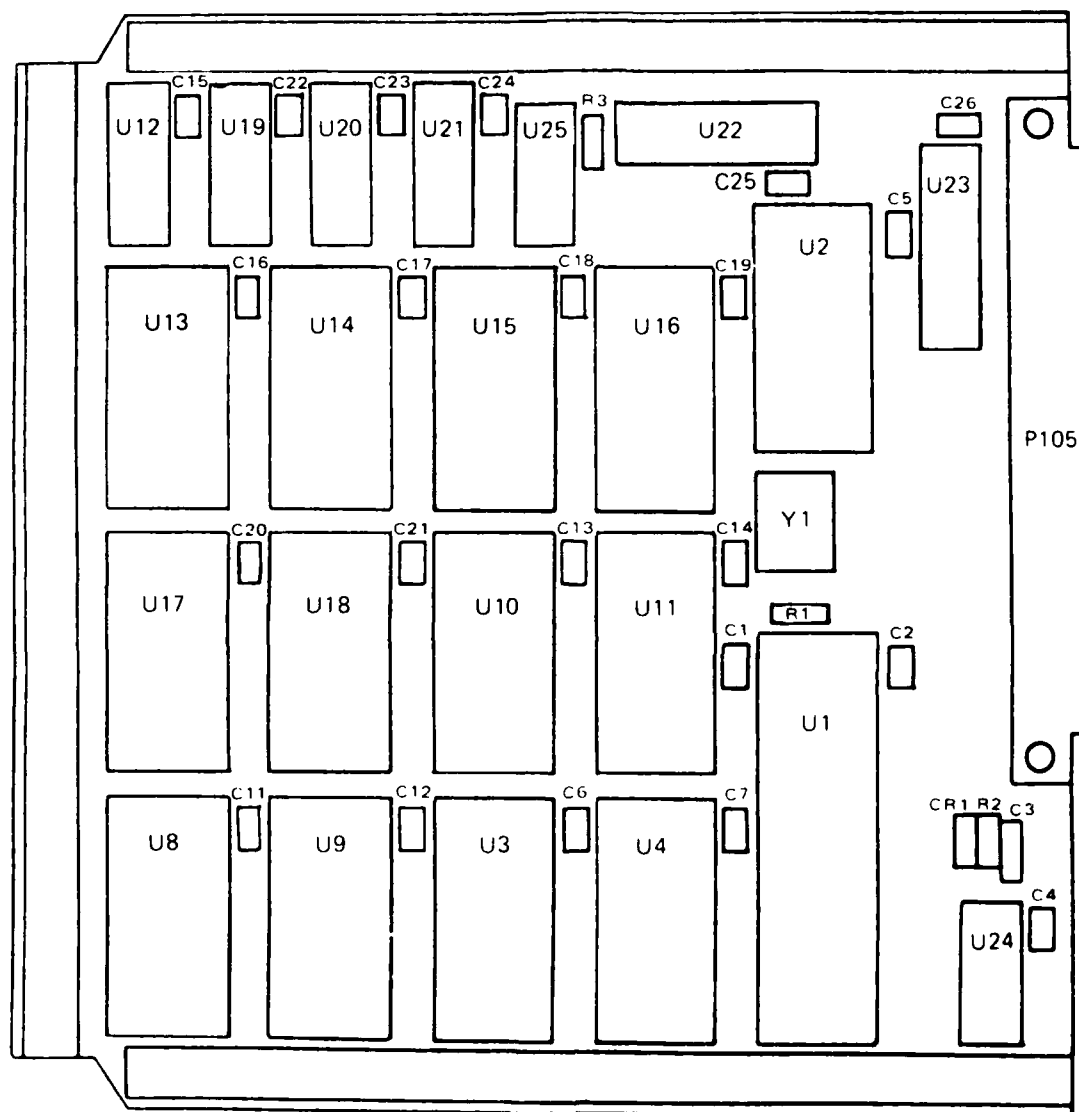


Figure 8 7. Master microprocessor assembly component layout.

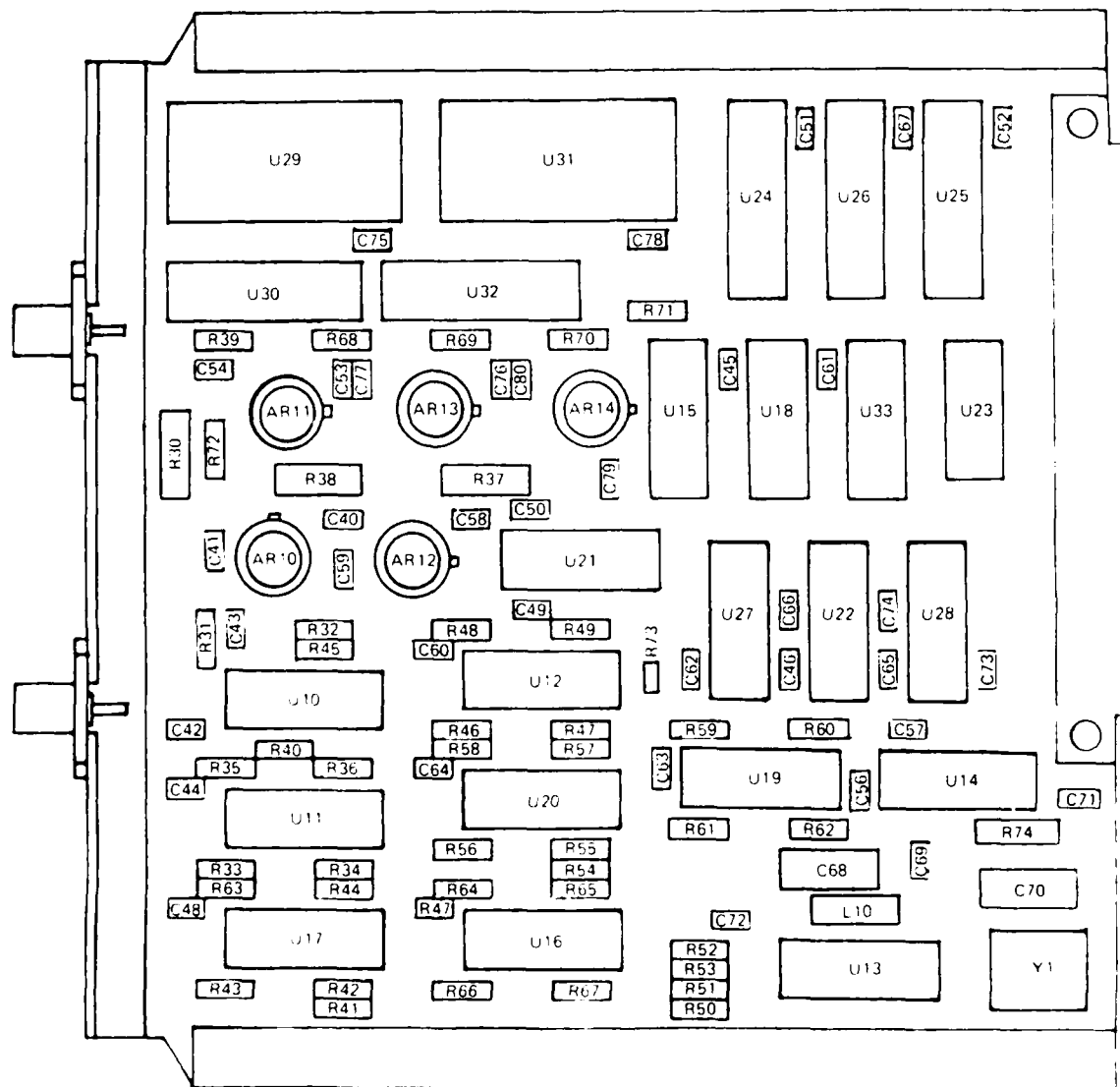


Figure 8 8. TPM threshold detector assembly component layout.

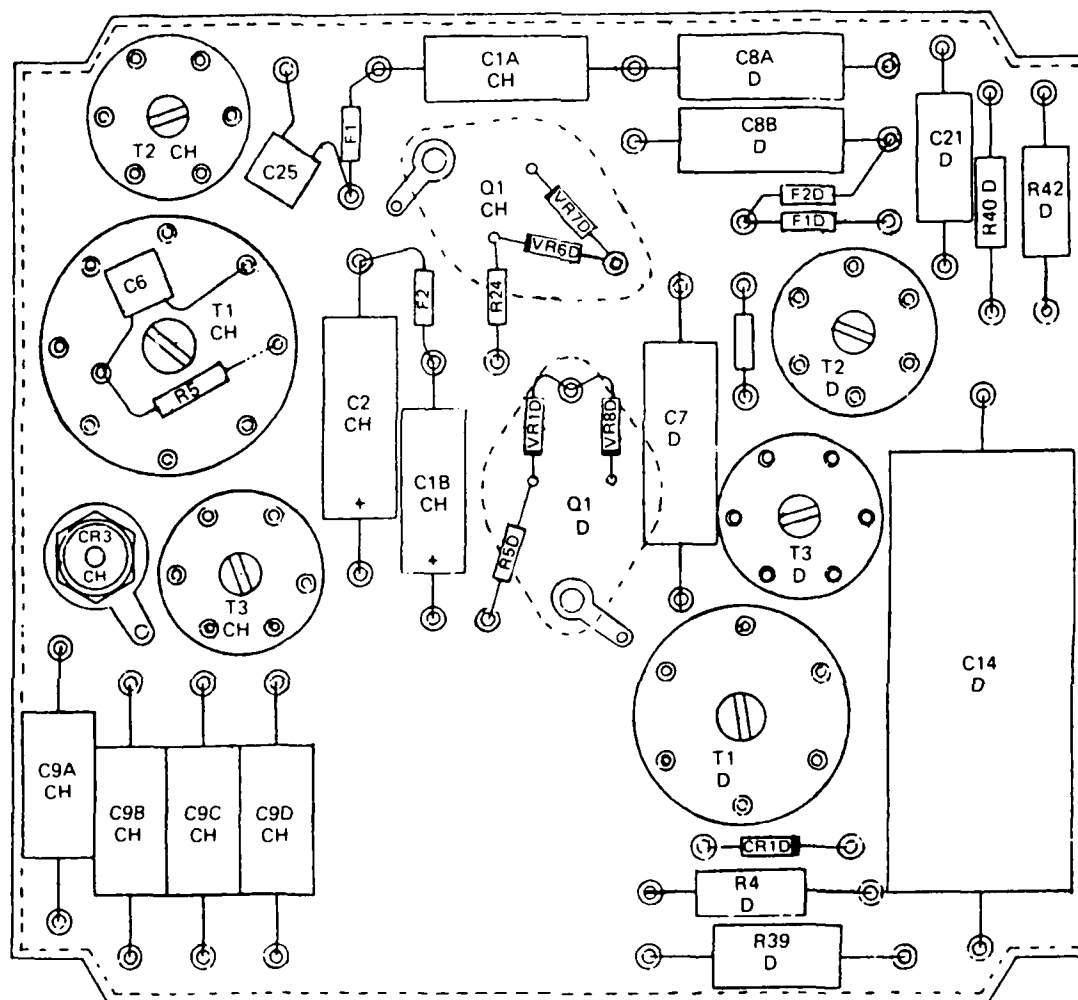


Figure 8-9. Plasma Generator Electronics (shelf 2) assembly component layout.

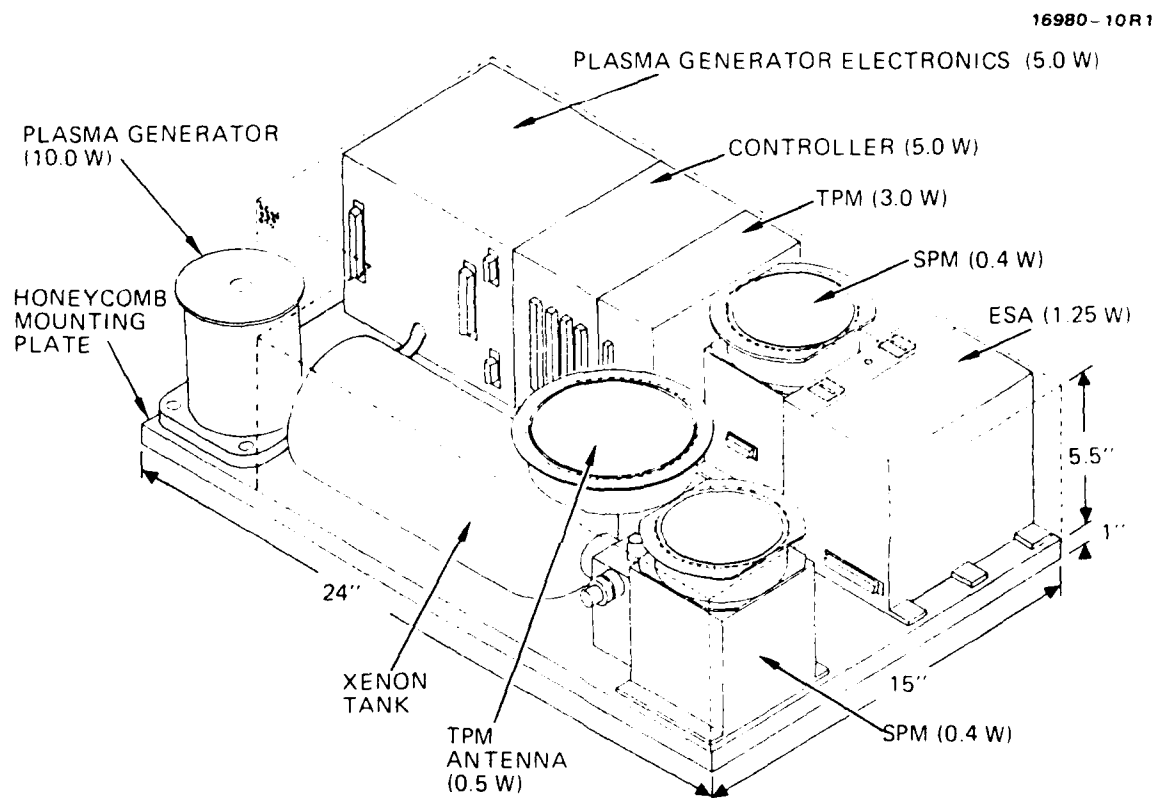


Figure 8-10. FMDS power dissipation map.

Two thermal cases are considered for these operating modes. For the first, the hot case, operating and environmental conditions are chosen to result in the highest system temperatures. The system is considered to be in the "operating" mode with a 43°C mounting surface temperature, and under a solar load at the End-of-Life (EOL). For the second case, the cold case, the mounting surface temperature is -13°C, there is no solar load, and the system is in the "monitoring" mode.

The TPM Threshold Detector, the Plasma Generator Electronics (Shelf 2), and the Master Microprocessor Assemblies are assumed to dissipate a worst case of 4.8, 11.4, and 0.3 W respectively. In actual practice, they will dissipate less power than this. The boundary temperatures for the TPM Threshold Detector Assembly are 54°C at the bottom bracket and 50°C at the top bracket. The boundary temperatures for the Plasma Generator Electronics and Master Microprocessor Assemblies are 57°C at the bottom bracket and 61°C at the top bracket. These boundary temperatures were calculated using the system thermal model for the hot case and are both (top and bottom) within 4°C of each other. Junction and case temperatures for the parts are compared to component derated temperatures per Hughes S&CG document number PA201.

### 8.3 ASSUMPTIONS

The following assumptions were made in the system analysis:

- 1) Off normal solar incidence (23.4°)
- 2) Unobstructed view of space
- 3) No concentration of solar load
- 4) Internal subassemblies painted black
- 5) Surface properties:

	<u>Emissivity</u>	<u>Absorption</u>
Radiator	0.8	0.1(BOL)/0.2(EOL)
MLI blanket	0.65	0.1(BOL)

- 6) Aluminum wall thickness:

Enclosure - 0.050 in.  
Electronics box - 0.050 in.



The following assumptions were made in the board analyses:

- 1) There is negligible thermal contact resistance between the board and its mounting bracket.
- 2) The copper planes extend throughout the board (except where cutouts occur) and under the area in contact with the mounting brackets - the latter point should not be overlooked with regard to its impact on board temperature deltas.
- 3) All component maximum allowable temperatures are taken to be 100°C for the Master Microprocessor Assembly.
- 4) The junction-to-case thermal resistance ( $\theta_{JC}$ ) for U1, U3-U11, and U19-U23 of the Master Microprocessor Assembly was assumed to be 80°C/W. The actual value was unknown at the time of analysis; however, this is a typical value for military approved dual-in-line packages.
- 5) The junction-to-case thermal resistances ( $\theta_{JC}$ ) for the TPM Threshold Detector Assembly are shown in Table 8-1.

#### 8.4 ANALYSIS METHOD

The system-level thermal model was shown in Figure 8-5 and represents a simplified version of the more detailed system nodal map as shown in Figure 8-11. Predicted temperatures at the nodes of Figure 8-11 were calculated using the CINDA thermal analyzer program available at Hughes.

The board analyses were performed using CINDA with preprocessing accomplished through the use of Hughes Product Analysis Laboratory's NEWT5 and ATDP programs. NEWT5 permits the digitized input of board and component position data, while ATDP automates certain phases of input and output table format.

#### 8.5 RESULTS

The system-level results are presented as curves of  $A_R$  (normalized radiator area) versus  $T_{HOT}$  and as curves of  $Q$  (heater dissipation in watts) versus  $T_{COLD}$  with  $A_R$  as a parameter. The variables  $T_{HOT}$  and  $T_{COLD}$  are taken at the top of the plasma generator electronics box, node 11 in Figure 8-11. This node was chosen to provide a reference electronics module mounting

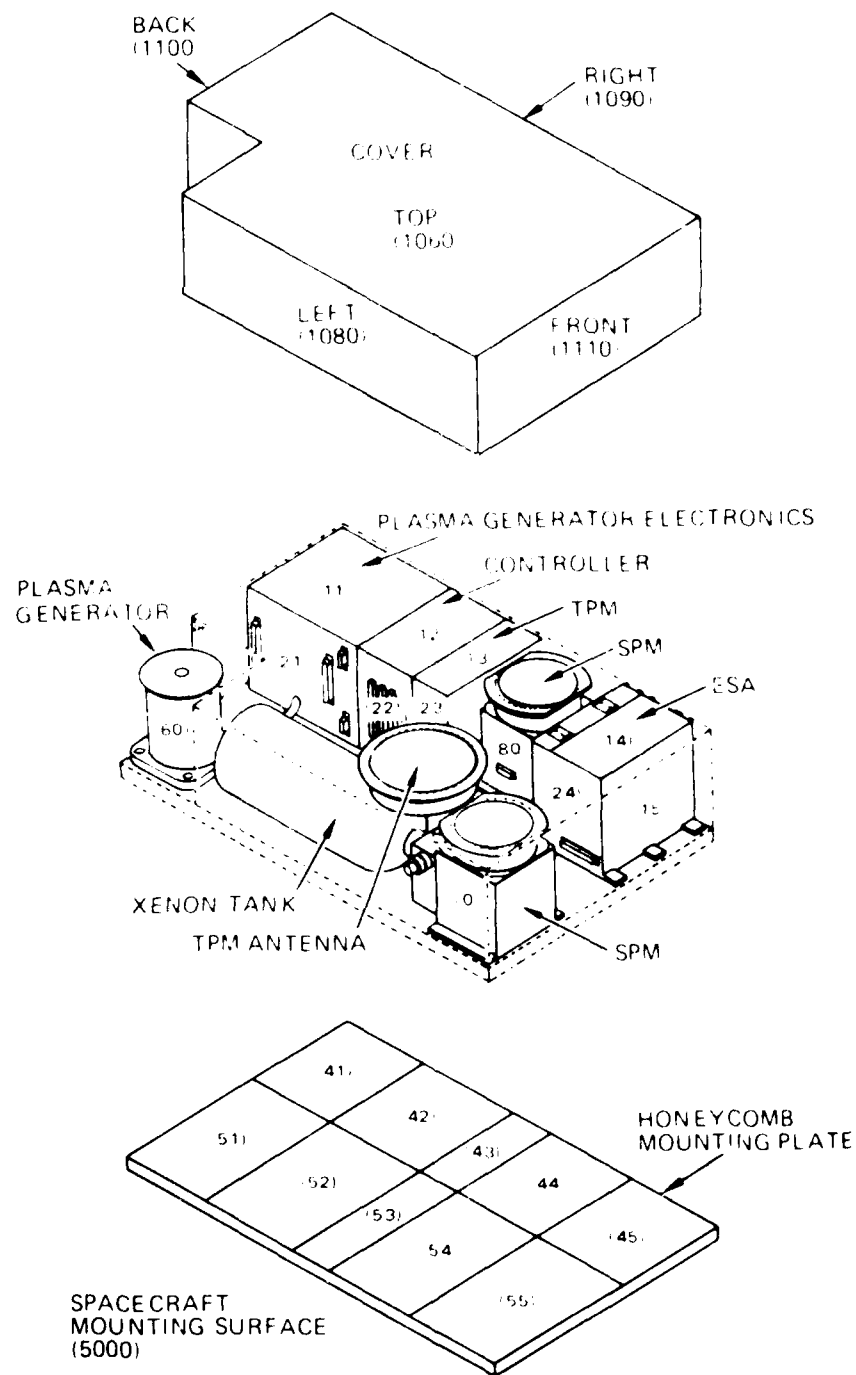


Figure 8-11. Detailed FMDS nodal map.

temperature. If this value is too high, then the electronic components will have high operating temperatures resulting in reduced reliability and shorter life time. The curves of Figure 8-12 are labeled as follows:

- C FMDS conductively connected (thermally) to the satellite with mounting surface temperatures of  $43^{\circ}\text{C}$  and  $-13^{\circ}\text{C}$ .
- R FMDS radiatively connected to the satellite with internal satellite subsystems at  $43^{\circ}\text{C}$  and  $-13^{\circ}\text{C}$ .
- I FMDS insulated from the satellite.

The connection referred to here is from the FMDS honeycomb mounting plate to the satellite as shown in Figures 8-5 and 8-11.

The radiator size  $A_R$  in Figure 8-12 was determined from the "hot case" by calculating the temperature  $T_{11}$  for which  $T_{11} = T_{HOT}$ . If the radiative area is less than this area then  $T_{11} > T_{HOT}$ ; if the area is greater then  $T_{11} < T_{HOT}$ .

All curves exhibit a drop in temperature as the radiator area increases. The slopes of the curves vary, with the insulated case showing the greatest variation in temperature with a change in radiator area. The conductive case provides the best thermal connection with the satellite and shows the least variation of  $T_{HOT}$  with a change in area.

The heater power in Figures 8-13 through 8-15, assumed to be distributed uniformly over the enclosure sides, was determined from the "cold case" with the radiator area as a given and calculating the node 11 temperature for which  $T_{11} = T_{COLD}$ . If the heater dissipation is greater, then  $T_{11} > T_{COLD}$ ; if the dissipation is less, then  $T_{11} < T_{COLD}$ .

Figures 8-13 through 8-15 plot curves of  $Q$  versus  $T_{COLD}$  for the conductive, radiative, and insulated cases respectively. Depending on the mounting arrangement, these curves can be used to estimate the heater value that would be required to keep component temperatures within a specified operating temperature range.

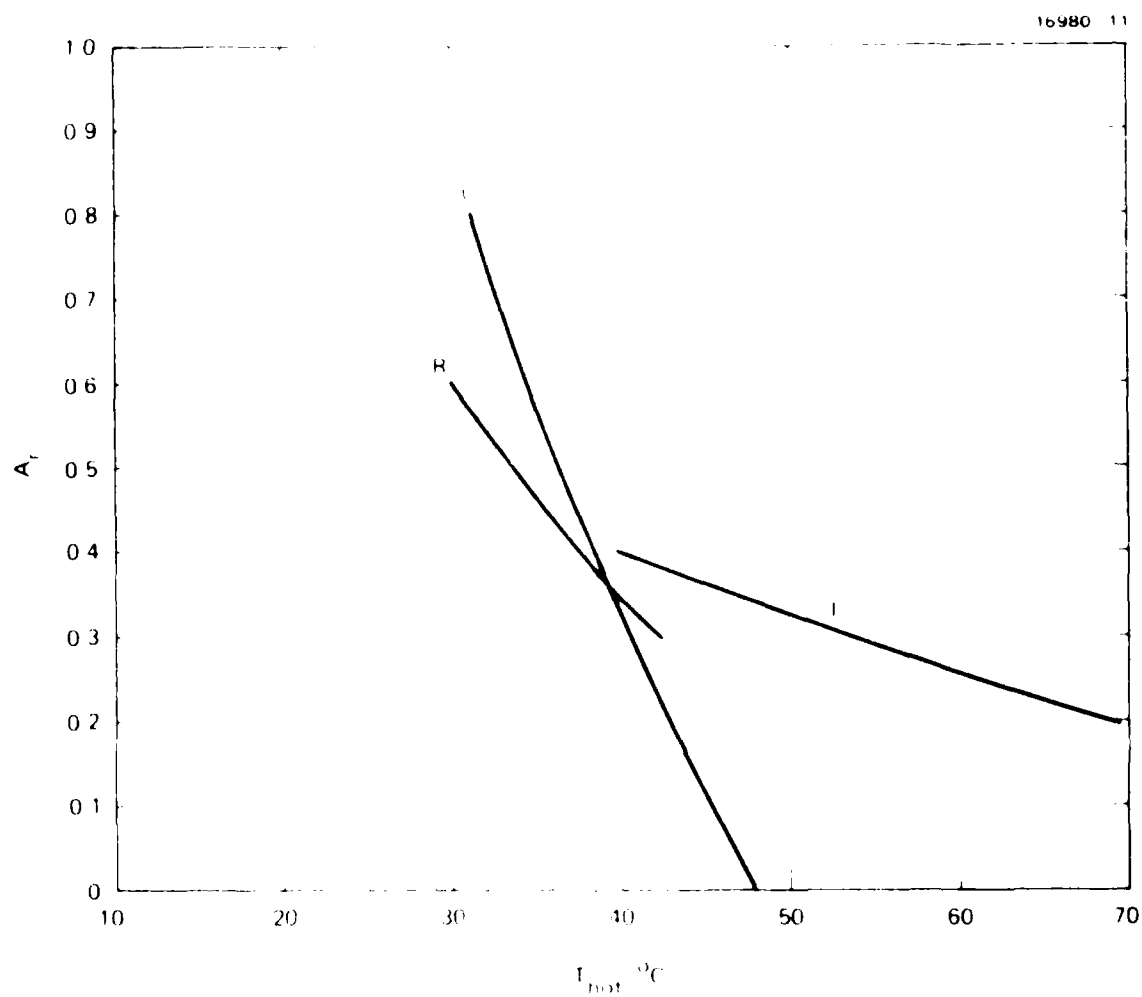


Figure 8 12 Normalized radiator area versus  $T_{HOT}$  for the conductive, radiative, and insulated connections with  $T_w = 43^{\circ}\text{C}$ .

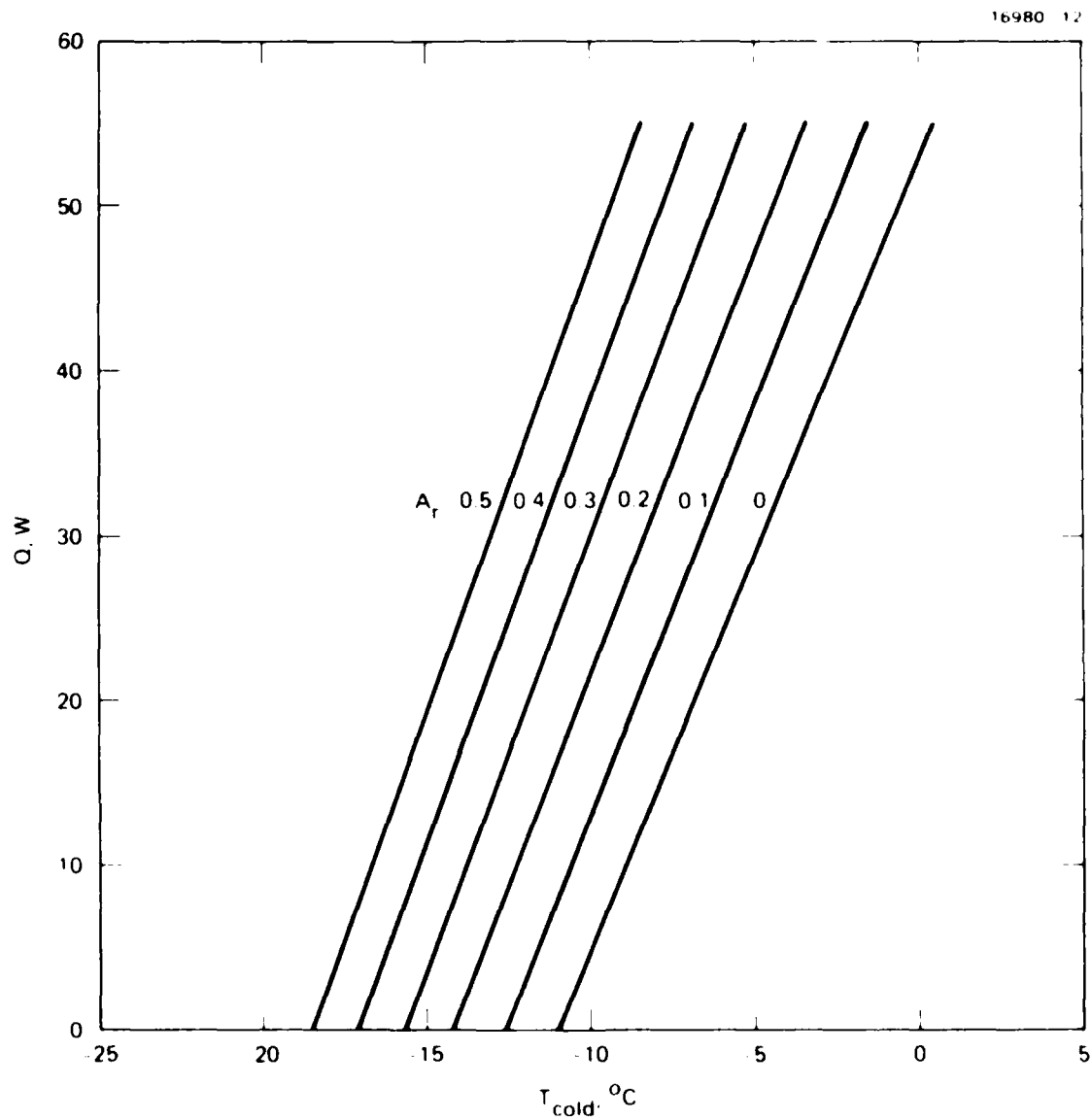


Figure 8 13. Heater power versus  $T_{\text{COLD}}$  for the conductive connection with  $T_{\text{H}} = 13^{\circ}\text{C}$ .

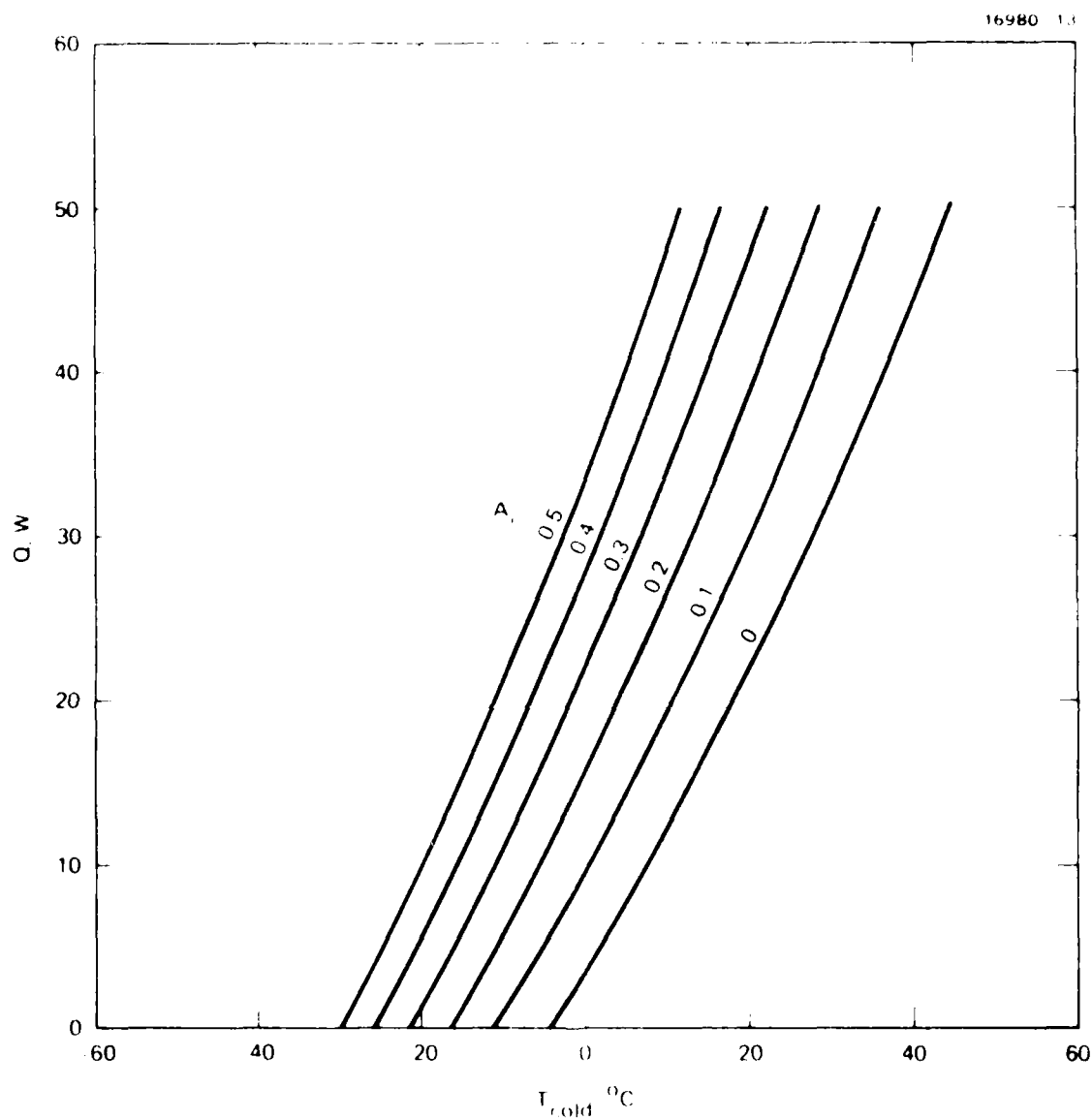


Figure 8-14. Heater power versus  $T_{\text{cold}}$  for the radiative connection with  $T_w = 13^{\circ}\text{C}$ .

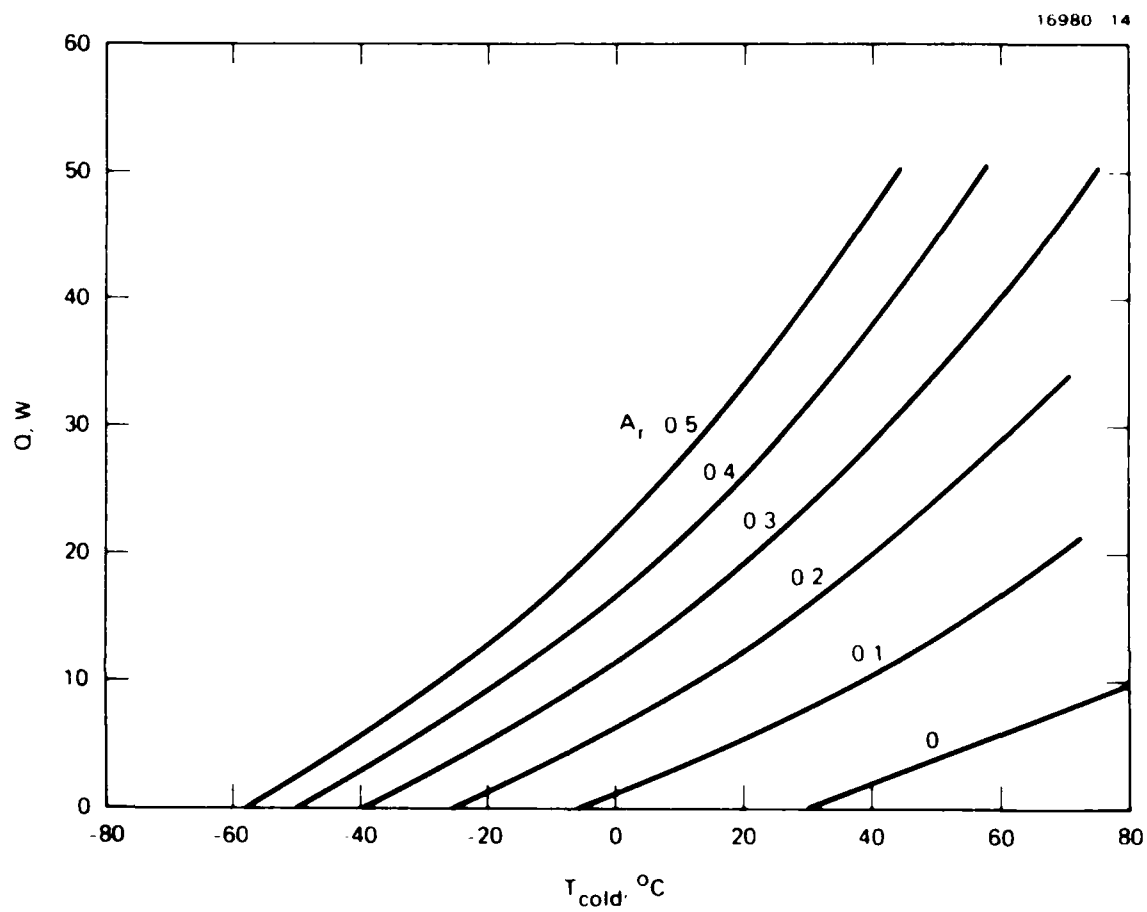


Figure 8-15. Heater power versus  $T_{cold}$  for the case where FMDS is insulated from the satellite.

Given the electronics box boundary temperatures for the "hot case," the three electronics assemblies were analyzed to provide board temperature maps for given component dissipations and mounting technique. The results of the analyses are presented in Tables 8-1 through 8-3. Table 8-1 lists the component case and junction temperatures for the TPM Threshold Detector Assembly. These results indicate that all components are operating below their maximum allowable operating temperature limit. The same thing can be said for the Plasma Generator Electronics (Shelf 2) Assembly listed in Table 8-2 and for the Master Microprocessor Assembly listed in Table 8-3.

## 8.6 FMDS SYSTEM DESIGN

From Figures 8-12 through 8-15, a radiator area ( $A_R$ ) and a maximum required heater power ( $Q$ ) can be determined that will allow the FMDS system to operate for any of the three mounting configurations (conductive, radiative, or insulated). The analysis of the three electronics assemblies shows that for a node 11 temperature (upper boundary of the Plasma Generator Electronics Assembly) of  $61^\circ\text{C}$ , that some of the TPM Threshold Detector Assembly component junction temperatures are within  $5^\circ\text{C}$  of the maximum allowed (Table 8-1). Therefore,  $T_{11}$  should be maintained at  $\leq 61^\circ\text{C}$  to keep the electronic components below an acceptable upper temperature limit.

Figure 8-12 shows that for  $A_R = 0.25$ ,  $T_{HOT}$  (which is really  $T_{11}$ ) will be  $\leq 61^\circ\text{C}$  for all three mounting configurations. If we choose  $A_R = 0.3$  to allow for some margin in the design, then  $T_{11}$  for the three mounting configurations will be:

C	$T_{11}$	$41^\circ\text{C}$
R	$T_{11}$	$43^\circ\text{C}$
I	$T_{11}$	$53^\circ\text{C}$

Minus  $24^\circ\text{C}$  is the lowest temperature that the system will be tested to; therefore,  $T_{11} = 24^\circ\text{C}$  is the coldest temperature that can be allowed and still guarantee that the system will function



Table 8 1. TPM Threshold Detector Assembly Steady State Component Operating Temperatures

CIRCUIT SYMBOL	PART NUMBER	THETA	POWER	MOUNTING		JUNCTION TEMP (DEG C)	MAXIMUM ALLOWABLE TEMP (DEG C)
		JC (DEG C/W)	(WATTS)	SURFACE TEMP (DEG C)	CASE TEMP (DEG C)		
U10	M38510/06301BEB	50.000	0.380	74.	81.	100.	105.
U11	M38510/06002BEB	50.000	0.100	71.	72.	77.	105.
U12	M38510/06002BEB	50.000	0.100	74.	76.	81.	105.
U13	M38510/10516/BEBJC	35.000	0.250	63.	65.	74.	105.
U14	M38510/06301BEB	50.000	0.380	73.	78.	97.	105.
U15	CD4040BD/3AR	50.000	0.002	71.	71.	71.	105.
U16	M38510/06101BEB	50.000	0.250	65.	70.	82.	105.
U17	M38510/10578/BEBJC	35.000	0.375	66.	73.	86.	105.
U18	CD4040BD/3AR	50.000	0.002	71.	71.	72.	105.
U19	M38510/06101BEB	50.000	0.250	73.	76.	89.	105.
U20	M38510/10578/BEBJC	35.000	0.375	73.	80.	93.	105.
U21	M38510/06302BEB	50.000	0.380	74.	81.	100.	105.
U22	M38510/06302BEB	50.000	0.380	75.	82.	101.	105.
U23	M38510R/17101BCB	50.000	0.001	70.	70.	70.	105.
U24	HS1-82008RH-8	50.000***	0.004	65.	65.	65.	105.
U25	HS1-82008RH-8	50.000***	0.004	64.	64.	64.	105.
U26	HS1-82008RH-8	50.000***	0.004	65.	65.	65.	105.
U27	M38510/06302BEB	50.000	0.380	75.	82.	101.	105.
U28	M38510/06302BEB	50.000	0.380	74.	81.	100.	105.
U29	M7 510R/17602BJB	40.000	0.004	62.	62.	62.	105.
U30	TRW5435**		0.001	66.	66.		105.
U31	M38510R/17602BJB	40.000	0.004	62.	62.	62.	105.
U32	TRW5435**		0.001	66.	66.		105.
U33	M38510R/05553BEB	50.000	0.001	71.	71.	71.	105.
Y1	909146-13		0.000	62.	62.		105.
L10	M39010/06BR33LR		0.000	67.	67.		105.
AR10	LM161H/883B	45.000	0.100	73.	77.	81.	105.
AR11	HS2-3530RH-8	45.000***	0.020	69.	70.	71.	105.
AR12	LM161H/883B	45.000	0.100	73.	77.	82.	105.
AR13	HS2-3530RH-8	45.000***	0.020	68.	69.	70.	105.
AR14	HS2-3530RH-8	45.000***	0.020	69.	70.	71.	105.
R30	RNO60H1500FR		0.013	71.	84.		110.
R31	RCR07G102JS		0.013	72.	87.		96.
R32	RCR07G511JS		0.013	73.	87.		96.
R33	RCR07G511JS		0.013	68.	82.		96.
R34	RCR07G511JS		0.013	68.	83.		96.
R35	RCR07G511JS		0.013	73.	85.		96.
R36	RCR07G511JS		0.013	73.	86.		96.
R37	RNO60H3162FR		0.013	72.	86.		110.
R38	RNO60H3162FR		0.013	71.	85.		110.
R39	RCR07G153JS		0.013	69.	83.		96.

NOTE: THE MAXIMUM ALLOWABLE TEMPERATURE IS THE UPPER LIMIT OF THE "ACCEPTABLE" TEMPERATURE REGION.

-- THIS COMPONENT IS A RESISTOR NETWORK AND DOES NOT HAVE A JUNCTION.

---  $\theta_{JC}$  WAS ASSUMED FOR THIS COMPONENT

(Continued)

Table 8-1. TPM Threshold Detector Assembly Steady  
State Component Operating Temperatures  
(continued)

CIRCUIT SYMBOL	PART NUMBER	THETA JC (DEG C/W)	POWER (WATTS)	MOUNTING		JUNCTION TEMP (DEG C)	MAXIMUM ALLOWABLE TEMP (DEG C)
				SURFACE TEMP (DEG C)	CASE TEMP (DEG C)		
R40	RCR07G511JS		0.013	73.	87.		95.
R41	RCR07G511JS		0.013	59.	73.		95.
R42	RCR07G511JS		0.013	59.	73.		95.
R43	RCR07G511JS		0.013	59.	73.		95.
R44	RCR07G511JS		0.013	68.	83.		95.
R45	RCR07G511JS		0.013	74.	88.		95.
R46	RCR07G511JS		0.013	73.	87.		95.
R47	RCR07G511JS		0.013	73.	87.		95.
R48	RCR07G511JS		0.013	74.	88.		95.
R49	RCR07G511JS		0.013	74.	88.		95.
R50	RCR07G511JS		0.013	58.	73.		95.
R51	RCR07G511JS		0.013	58.	73.		95.
R52	RCR07G511JS		0.013	63.	78.		95.
R53	RCR07G511JS		0.013	63.	78.		95.
R54	RCR07G511JS		0.013	68.	83.		95.
R55	RCR07G511JS		0.013	68.	83.		95.
R56	RCR07G511JS		0.013	68.	83.		95.
R57	RCR07G511JS		0.013	73.	87.		95.
R58	RCR07G511JS		0.013	73.	87.		95.
R59	RCR07G511JS		0.013	73.	87.		95.
R60	RCR07G511JS		0.013	73.	87.		95.
R61	RCR07G511JS		0.013	70.	83.		95.
R62	RCR07G511JS		0.013	70.	83.		95.
R63	RCR07G511JS		0.013	68.	82.		95.
R64	RCR07G511JS		0.013	68.	83.		95.
R65	RCR07G511JS		0.013	68.	83.		95.
R66	RCR07G511JS		0.013	59.	73.		95.
R67	RCR07G511JS		0.013	58.	73.		95.
R68	RCR07G243JS		0.013	69.	83.		95.
R69	RCR07G394JS		0.013	69.	83.		95.
R70	RCR07G243JS		0.013	69.	83.		95.
R71	RCR07G394JS		0.013	65.	80.		95.
R72	RCR07G394JS		0.013	71.	84.		95.
R73	RCR07G511JS		0.013	73.	88.		95.
R74	RNO60H4021		0.001	69.	69.		119.
O40	M39014/01-1553		0.000	71.	71.		100.
O41	M39014/01-1553		0.000	72.	72.		100.
O42	M39014/01-1553		0.000	71.	71.		100.
O43	M39014/01-1553		0.000	73.	73.		100.
O44	M39014/01-1553		0.000	70.	70.		100.
O45	M39014/01-1553		0.000	69.	69.		100.

NOTE: THE MAXIMUM ALLOWABLE TEMPERATURE IS THE UPPER LIMIT  
OF THE "ACCEPTABLE" TEMPERATURE REGION.

(Continued)

Table 8 1. TPM Threshold Detector Assembly Steady  
State Component Operating Temperatures  
(continued)

CIRCUIT SYMBOL	PART NUMBER	THETA JC (DEG C/W)	POWER (WATTS)	MOUNTING SURFACE TEMP (DEG C)	CASE TEMP (DEG C)	JUNCTION TEMP (DEG C)	MAXIMUM ALLOWABLE TEMP (DEG C)
O46	M39014/01-1553		0.000	75.	75.		100.
O48	M39014/01-1553		0.000	67.	67.		100.
O49	M39014/01-1553		0.000	74.	74.		100.
C50	M39014/01-1553		0.000	72.	72.		100.
C51	M39014/01-1553		0.000	62.	62.		100.
C52	M39014/01-1553		0.000	61.	61.		100.
C53	M39014/01-1553		0.000	69.	69.		100.
C54	M39014/01-1553		0.000	69.	69.		100.
C56	M39014/01-1553		0.000	70.	70.		100.
C57	M39014/01-1553		0.000	73.	73.		100.
C58	M39014/01-1553		0.000	72.	72.		100.
C59	M39014/01-1553		0.000	73.	73.		100.
O60	M39014/01-1553		0.000	73.	73.		100.
O61	M39014/01-1553		0.000	68.	68.		100.
O62	M39014/01-1553		0.000	73.	73.		100.
O63	M39014/01-1553		0.000	72.	72.		100.
O64	M39014/01-1553		0.000	68.	68.		100.
O65	M39014/01-1553		0.000	74.	74.		100.
O66	M39014/01-1553		0.000	75.	75.		100.
O67	M39014/01-1553		0.000	62.	62.		100.
O68	908535-1		0.000	67.	67.		100.
O69	M39014/01-1553		0.000	66.	66.		100.
C70	908535-1		0.000	65.	65.		100.
C71	M39014/01-1553		0.000	69.	69.		100.
C72	M39014/01-1553		0.000	63.	63.		100.
C73	M39014/01-1553		0.000	71.	71.		100.
C74	M39014/01-1553		0.000	74.	74.		100.
C75	M39014/01-1553		0.000	66.	66.		100.
C76	M39014/01-1553		0.000	69.	69.		100.
C77	M39014/01-1553		0.000	69.	69.		100.
C78	M39014/01-1553		0.000	65.	65.		100.
C79	M39014/01-1553		0.000	72.	72.		100.
O80	M39014/01-1553		0.000	69.	69.		125.

TOTAL OF PART DISSIPATIONS:

4.841 WATTS

AVERAGE JUNCTION TEMPERATURE:

79.5 DEG C

NOTE: THE MAXIMUM ALLOWABLE TEMPERATURE IS THE UPPER LIMIT  
OF THE 'ACCEPTABLE' TEMPERATURE REGION

Table 8 2. Plasma Generator Electronics (Shelf 2) Assembly  
Steady State Component Operating Temperatures

CIRCUIT SYMBOL	PART NUMBER	THETA JC (DEG C/W)	POWER (WATTS)	MOUNTING SURFACE TEMP (DEG C)	CASE TEMP (DEG C)	JUNCTION TEMP (DEG C)	MAXIMUM ALLOWABLE TEMP (DEG C)
C1ACH	M39006/22-0568		0.100	61.	61.		85.
C1BCH	M39006/22-0568		0.100	65.	65.		85.
C2CH	M83421/01-2255S		0.000	65.	65.		85.
O6CH	M39014/01-1523		0.000	78.	78.		125.
C7D	M83421/01-2255S		0.000	63.	63.		85.
O8AD	M39006/22-0568		0.100	61.	61.		85.
O8BD	M39006/22-0568		0.100	61.	61.		85.
O9ACH	M39006/22-0554		0.100	62.	63.		85.
O9BCH	M39006/22-0554		0.100	62.	63.		85.
O9OCH	M39006/22-0554		0.100	62.	63.		85.
O9DCH	M39006/22-0554		0.100	62.	63.		85.
C14D	M83421/01-4317S		0.000	61.	61.		85.
C21D	M39003/01-3094		0.000	61.	61.		85.
C22D	M39014/02-1310		0.000	62.	62.		125.
C25CH	M39014/02-1310		0.000	61.	61.		125.
OR1D	JANTXVSDRIM		0.400	60.	66.		105.
OR3CH	JANTXV1N5816	1.500	2.000	69.	73.	76.	105.
F1CH	988244-13		0.000	61.	61.		85.
F2CH	988244-13		0.000	65.	65.		85.
F1D	988244-13		0.000	61.	61.		85.
F2D	988244-13		0.000	61.	61.		85.
Q1CH	JANTXV2N6766	0.830	2.000	61.	69.	70.	105.
Q1D	JANTXV2N6766	0.830	0.500	63.	65.	66.	105.
R4D	RCR32G511JS		0.000	57.	57.		98.
R5CH	RCR20G221JS		0.250	78.	80.		98.
R5D	RCR07G100JS		0.000	63.	63.		98.
R24CH	RCR07G100JS		0.000	63.	63.		98.
R39D	RCR42G223JS		0.050	57.	57.		98.
R40D	RWR80S1R00FR		0.000	61.	61.		140.
R42D	RCR32G101JS		0.000	61.	61.		98.
T1CH	1099467		4.000	71.	78.		85.
T1D	1099463		1.000	62.	65.		85.
T2CH	1099460		0.100	61.	61.		85.
T2D	1099460		0.100	62.	63.		85.
T3CH	1099460		0.100	69.	69.		85.
T3D	1099460		0.100	62.	63.		85.
VR1D	JANTXV1N4470		0.000	63.	63.		105.
VR6CH	JANTXV1N4470		0.000	61.	61.		105.
VR7CH	JANTXV1N4470		0.000	61.	61.		105.
VR8D	JANTXV1N4470		0.000	63.	63.		105.

TOTAL OF PART DISSIPATIONS: 11.400 WATTS  
AVERAGE JUNCTION TEMPERATURE: 70.5 DEG C

NOTE: THE MAXIMUM ALLOWABLE TEMPERATURE IS THE UPPER LIMIT  
OF THE 'ACCEPTABLE' TEMPERATURE REGION

Table 8-3. Master Microprocessor Assembly Steady State Component Operating Temperatures

CIRCUIT SYMBOL	PART NUMBER	POWER (WATTS)	MOUNTING SURFACE TEMP (DEG C)	CASE TEMP (DEG C)	JUNCTION TEMP (DEG C)	MAXIMUM ALLOWABLE TEMP (DEG C)
U1	HS1-80C85RH/B	0.018	67.	67.	69. •	100.
U2	CD4508	0.004	66.	67.	67.	100.
U3	MA6116SOS	0.100	69.	72.	80. •	100.
U4	MA6116SOS	0.100	69.	72.	80. •	100.
U8	HS1-6641RH/B	0.005	68.	68.	68. •	100.
U9	HS1-6641RH/B	0.005	67.	67.	68. •	100.
U10	HS1-6641RH/B	0.005	67.	67.	68. •	100.
U11	HS1-6641RH/B	0.005	67.	67.	68. •	100.
U12	CD40175	0.000	66.	66.	66.	100.
U13	SA2999-1	0.005	67.	67.	68.	100.
U14	SA2999-1	0.005	67.	67.	67.	100.
U15	SA2999-1	0.005	67.	67.	67.	100.
U16	SA2999-1	0.005	67.	67.	67.	100.
U17	SA2999-1	0.005	68.	68.	68.	100.
U18	SA2999-1	0.005	67.	67.	68.	100.
U19	HS1-54C138RH/B	0.002	66.	66.	67. •	100.
U20	HS1-54C138RH/B	0.002	66.	66.	67. •	100.
U21	HS1-54C138RH/B	0.002	66.	66.	66. •	100.
U22	HS1-82C08RH/B	0.004	66.	66.	67. •	100.
U23	HS1-82C08RH/B	0.004	66.	66.	67. •	100.
U24	CD4093	0.001	66.	66.	66.	100.
U25	CD4081	0.001	66.	66.	66.	100.
CR1	JANTX1N3600	0.000	66.	66.	66.	100.
R1	RESISTOR	0.000	67.	67.		100.
R2	RESISTOR	0.000	66.	66.		100.
R3	RESISTOR	0.000	66.	66.		100.
Y1	CRYSTAL	0.000	67.	67.		100.
C1	CAPACITOR	0.000	67.	67.		100.
C2	CAPACITOR	0.000	67.	67.		100.
C3	CAPACITOR	0.000	66.	66.		100.
C4	CAPACITOR	0.000	66.	66.		100.
C5	CAPACITOR	0.000	66.	66.		100.
C6	CAPACITOR	0.000	68.	68.		100.
C7	CAPACITOR	0.000	67.	67.		100.
C11	CAPACITOR	0.000	67.	67.		100.
C12	CAPACITOR	0.000	67.	67.		100.
C13	CAPACITOR	0.000	67.	67.		100.
C14	CAPACITOR	0.000	67.	67.		100.
C15	CAPACITOR	0.000	66.	66.		100.
C16	CAPACITOR	0.000	66.	66.		100.
C17	CAPACITOR	0.000	66.	66.		100.
C18	CAPACITOR	0.000	66.	66.		100.
C19	CAPACITOR	0.000	66.	66.		100.
C20	CAPACITOR	0.000	67.	67.		100.
C21	CAPACITOR	0.000	67.	67.		100.
C22	CAPACITOR	0.000	66.	66.		100.
C23	CAPACITOR	0.000	66.	66.		100.
C24	CAPACITOR	0.000	66.	66.		100.
C25	CAPACITOR	0.000	66.	66.		100.
C26	CAPACITOR	0.000	66.	66.		100.

• JUNCTION TEMPERATURE APPROXIMATED BASED ON  $\theta_{JC} = 80^{\circ}\text{C/W}$   
TOTAL OF PART DISIPATIONS 0.288 W

properly when turned ON. With the system turned completely OFF, the electronic components will come to equilibrium at  $-24^{\circ}\text{C}$  and then start to warm up immediately when turned ON. Figures 8-13 through 8-15 assume that the system is in the "monitoring" mode and dissipating 10.5 W. Under this condition with  $A_R = 0.3$ , the heater powers required to keep  $T_{11} (T_{\text{COLD}}) \geq -24^{\circ}\text{C}$  for the three mounting configurations are:

C (Figure 8-13) -  $Q = <0.0 \text{ W}$  (i.e., heater not required)

R (Figure 8-14) -  $Q = <0.0 \text{ W}$  (i.e., heater not required)

I (Figure 8-15) -  $Q = 4.0 \text{ W}$ .

The heater powers required to keep  $T_{11} \geq -24^{\circ}\text{C}$  with  $A_R = 0.3$  when the system is completely OFF, can be determined from Figures 8-13 through 8-15 by extrapolating the curves to the point at which they intersect the value of  $-24^{\circ}\text{C}$  and then adding 10.5 W to the value obtained (because the curves were calculated for the "monitoring" mode in which 10.5 W is dissipated). This results in:

C (Figure 8-13) -  $Q = <0.0 \text{ W}$  (i.e., heater not required)

R (Figure 8-14) -  $Q = 8.5 \text{ W}$

I (Figure 8-15) -  $Q = 14.5 \text{ W}$ .

The FMDS system will be cold soaked during environmental qualification at  $-24^{\circ}\text{C}$  and therefore its operation after being exposed to colder temperatures will not be guaranteed. However, the electronic components themselves have storage temperature ratings of  $-65^{\circ}\text{C}$ . The heater powers required to keep  $T_{11} \geq -65^{\circ}\text{C}$  can be estimated for the three cases (again by extrapolation) as:

C (Figure 8-13) -  $Q = <0.0 \text{ W}$  (i.e., heater not required)

R (Figure 8-14) -  $Q = <0.0 \text{ W}$  (i.e., heater not required)

I (Figure 8-15) -  $Q = 6.0 \text{ W}$ .

The above discussion leads to a FMDS system thermal design where 30% of the FMDS cover ( $A_R = 0.3$ ) is covered with radiator to keep the system cool and a 15 W heater is included to keep the system warm. This design will work for any one of the three mounting configurations (conductive, radiative, or insulated).

## 8.7 DISCUSSION AND RECOMMENDATIONS

It should be noted that the data presented in Figures 8-12 through 8-15 use one node temperature ( $T_{11}$ ) to represent the temperature of a typical electronics mounting surface within the system. A detailed temperature map of the system is provided by the CINDA computer run.

The following factors can influence the temperatures presented in this report:

- a) Host vehicle and mounting - effects of solar concentration, shading, etc.
- b) Launch and transport environment - worst case conditions might be encountered in transport.
- c) Dissipation and mode of operation - revised mission profile or operating experience might change these.
- d) Transient effects - post eclipse bus voltage can increase due to increased solar cell efficiency at low temperatures.

It is recommended but not required that bonding be used with all dissipating components on the TPM Threshold Detector Assembly and the Master Microprocessor Assembly. It is required and was assumed in the analysis that bonding (HP16-103 Type 13 is recommended) is used for all dissipating components on the Plasma Generator Electronics (Shelf 2) Assembly.

When the FMDS is integrated with a vehicle, emphasis should be placed on an understanding of items a-d above. A careful evaluation of these, keeping in mind the choice of satellite and launch mode, will determine the applicability of the present data and curves for the particular application. If significant solar concentration, shading, changes in dissipation, etc., occur, the computer model should be updated to reflect these changes.

## SECTION 9

### CONCLUSIONS

The Flight Model Discharge System (FMDS) Program has completed its third year with no technical problems that will preclude its successful completion. A breadboard plasma generator has successfully demonstrated the required lifetime necessary to meet FMDS requirements and no contamination problems from it are anticipated. The system thermal analyses have been completed and revealed no thermal problems.



## REFERENCES

1. R.R. Robson, W.S. Williamson, and J. Santoru, "Flight model discharge system scientific report no. 2," AFGL-TR-86-0036, February 1986. ADA169423
2. J.C. Sturman, "Development and design of three monitoring instruments for spacecraft charging," NASA Technical Paper 1800, 1981.
3. E.R. Moog and M.B. Webb, "Xenon and krypton adsorption on palladium (100)," Surface Science 148, pp. 338-370, 1984.
4. Multiwire/West Division Kollmorgen Corp.  
3901 East LaPalma Ave.  
Anaheim, CA 92807

END

12-87

DTIC